Chapter 4

Absorption and Scattering by a Sphere

Perhaps the most important exactly soluble problem in the theory of absorption and scattering by small particles is that for a sphere of arbitrary radius and refractive index. Although the formal solution to this problem has been available for many years, only since the advent of large digital computers has it been a practical means for detailed computations. In 1908, Gustav Mie developed the theory in an effort to understand the varied colors in absorption and scattering exhibited by small colloidal particles of gold suspended in water. About the same time Peter Debye considered the problem of the radiation pressure exerted on small particles in space. Debye's work, which was the subject of his doctoral dissertation, is one of the first applications of the theory to an astrophysical problem. Neither Mie nor Debye was the first to construct a solution to the sphere problem; however, establishing who precisely was the first is not an easy task, although Lorenz is a strong contender for this honor. Without trying to establish historical precedents, we shall accept the most common term, the Mie theory. A good concise but thorough treatment of the history of the sphere problem is given in Kerker (1969, pp. 54–59).

The mathematical basis of the Mie theory is the subject of this chapter. Expressions for absorption and scattering cross sections and angle-dependent scattering functions are derived; reference is then made to the computer program in Appendix A, which provides for numerical calculations of these quantities. This is the point of departure for a host of applications in several fields of applied science, which are covered in more detail in Part 3. The mathematics, divorced from physical phenomena, can be somewhat boring. For this reason, a few illustrative examples are sprinkled throughout the chapter. These are just appetizers to help maintain the reader's interest; a fuller meal will be served in Part 3.

Whereas the mathematics of the Mie theory is straightforward, if somewhat cumbersome, the physics of the interaction of an electromagnetic wave with a sphere is extremely complicated. It is a relatively easy matter to write the infinite series expansions of the electromagnetic fields at all points of space. It is an even easier matter these days to produce great reams of output from Mie computations. A more difficult task, however, is to visualize the fields, to

categorize the significant electromagnetic modes inside and outside the sphere, and to acquire some intuitive feeling for how a sphere of given size and optical properties absorbs and scatters light.

On the one hand, there are those who scoff at the use of the Mie theory to describe any properties of nonspherical particles, the type of particles that are likely to inhabit planetary atmospheres and the interstellar medium; on the other hand, there are those who unquestioningly use Mie theory for any and every aspect of light interaction with such particles. Neither attitude is enlightened. The Mie theory, limited though it may be, does provide a first-order description of optical effects in nonspherical particles, and it correctly describes many small-particle effects that are not intuitively obvious. For example, we shall see in Chapter 11, where we consider nonspherical particles, that the sphere solution is an excellent guide to the changes that occur when absorption increases or size dispersion changes. Therefore, our approach will be to explore fully the Mie theory and the optical effects it describes and then, in succeeding chapters, to critically examine its failings in dealing with nonspherical particles.

4.1 SOLUTIONS TO THE VECTOR WAVE EQUATIONS

We showed in Chapter 3 that a physically realizable time-harmonic electromagnetic field $(\mathbf{E}, \mathbf{H})$ in a linear, isotropic, homogeneous medium must satisfy the wave equation

$$\nabla^2\mathbf{E} + k^2\mathbf{E} = 0, \qquad \nabla^2\mathbf{H} + k^2\mathbf{H} = 0,$$

where $k^2 = \omega^2\varepsilon\mu$, and be divergence-free

$$\nabla \cdot \mathbf{E} = 0, \qquad \nabla \cdot \mathbf{H} = 0.$$

In addition, $\mathbf{E}$ and $\mathbf{H}$ are not independent:

$$\nabla \times \mathbf{E} = i\omega\mu\mathbf{H}, \qquad \nabla \times \mathbf{H} = -i\omega\varepsilon\mathbf{E}.$$

Suppose that, given a *scalar* function ψ and an arbitrary *constant* vector $\mathbf{c}$, we construct a *vector* function $\mathbf{M}$:

$$\mathbf{M} = \nabla \times (\mathbf{c}\psi).$$

The divergence of the curl of any vector function vanishes:

$$\nabla \cdot \mathbf{M} = 0.$$

If we use the vector identities

$$\nabla \times (\mathbf{A} \times \mathbf{B}) = \mathbf{A}(\nabla \cdot \mathbf{B}) - \mathbf{B}(\nabla \cdot \mathbf{A}) + (\mathbf{B} \cdot \nabla)\mathbf{A} - (\mathbf{A} \cdot \nabla)\mathbf{B},$$

$$\nabla(\mathbf{A} \cdot \mathbf{B}) = \mathbf{A} \times (\nabla \times \mathbf{B}) + \mathbf{B} \times (\nabla \times \mathbf{A}) + (\mathbf{B} \cdot \nabla)\mathbf{A} + (\mathbf{A} \cdot \nabla)\mathbf{B},$$

we obtain

$$\nabla^2\mathbf{M} + k^2\mathbf{M} = \nabla \times [\mathbf{c}(\nabla^2\psi + k^2\psi)].$$

Therefore, **M** satisfies the *vector* wave equation if ψ is a solution to the *scalar* wave equation

$$\nabla^2\psi + k^2\psi = 0.$$

We may also write $\mathbf{M} = -\mathbf{c} \times \nabla\psi$, which shows that **M** is perpendicular to **c**. Let us construct from **M** another vector function

$$\mathbf{N} = \frac{\nabla \times \mathbf{M}}{k}$$

with zero divergence, which also satisfies the vector wave equation

$$\nabla^2\mathbf{N} + k^2\mathbf{N} = 0.$$

We also have

$$\nabla \times \mathbf{N} = k\mathbf{M}.$$

Therefore, **M** and **N** have all the required properties of an electromagnetic field: they satisfy the vector wave equation, they are divergence-free, the curl of **M** is proportional to **N**, and the curl of **N** is proportional to **M**. Thus, the problem of finding solutions to the field equations reduces to the comparatively simpler problem of finding solutions to the scalar wave equation. We shall call the scalar function ψ a *generating function* for the *vector harmonics* **M** and **N**; the vector **c** is sometimes called the *guiding* or *pilot* vector.

The choice of generating functions is dictated by whatever symmetry may exist in the problem. In this chapter we are interested in scattering by a sphere; therefore, we choose functions ψ that satisfy the wave equation in spherical polar coordinates r, θ, ϕ (Fig. 4.1). The choice of pilot vector is somewhat less obvious. We could choose some arbitrary vector **c**. However, if we take

$$\mathbf{M} = \nabla \times (\mathbf{r}\psi), \tag{4.1}$$

where **r** is the radius vector, then **M** is a solution to the vector wave equation in *spherical polar coordinates*. In problems involving spherical symmetry, therefore, we shall take **M** given in (4.1) and the associated **N** as our fundamental solutions to the field equations. Note that **M** is everywhere tangential to any sphere $|\mathbf{r}|$ = constant (i.e., $\mathbf{r} \cdot \mathbf{M} = 0$).

The scalar wave equation in spherical polar coordinates is

$$\frac{1}{r^2}\frac{\partial}{\partial r}\left(r^2\frac{\partial\psi}{\partial r}\right) + \frac{1}{r^2\sin\theta}\frac{\partial}{\partial\theta}\left(\sin\theta\frac{\partial\psi}{\partial\theta}\right) + \frac{1}{r^2\sin\theta}\frac{\partial^2\psi}{\partial\phi^2} + k^2\psi = 0. \tag{4.2}$$

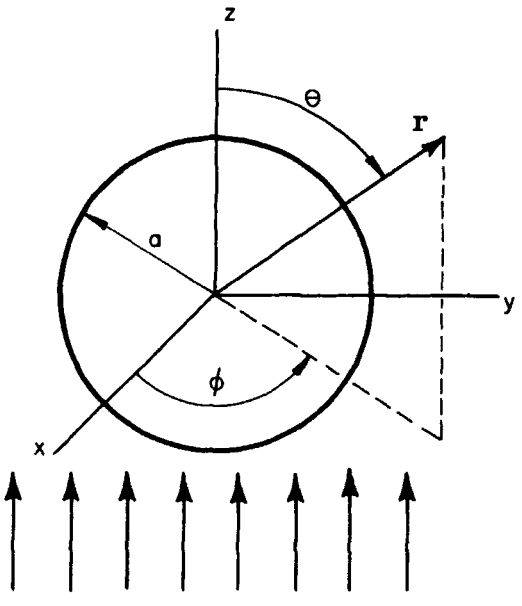

Figure 4.1 Spherical polar coordinate system centered on a spherical particle of radius a.

We seek particular solutions to (4.2) of the form

$$\psi(r, \theta, \phi) = R(r)\Theta(\theta)\Phi(\phi),$$

which when substituted into (4.2) yield the three separated equations:

$$\frac{d^2\Phi}{d\phi^2} + m^2\Phi = 0, \tag{4.3}$$

$$\frac{1}{\sin\theta}\frac{d}{d\theta}\left(\sin\theta\frac{d\Theta}{d\theta}\right) + \left[n(n+1) - \frac{m^2}{\sin^2\theta}\right]\Theta = 0, \tag{4.4}$$

$$\frac{d}{dr}\left(r^2\frac{dR}{dr}\right) + [k^2r^2 - n(n+1)]R = 0, \tag{4.5}$$

where the *separation constants* m and n are determined by subsidiary conditions that ψ must satisfy. We first note that if, for a given m, Φ_m is a solution to (4.3), then Φ_{-m} is not a linearly independent solution. The linearly independent solutions are

$$\Phi_e = \cos m\phi, \qquad \Phi_o = \sin m\phi,$$

where subscripts e and o denote *even* and *odd*. We require that ψ be a

single-valued function of the azimuthal angle ϕ:

$$\lim_{\nu \to 2\pi} \psi(\phi + \nu) = \psi(\phi) \tag{4.6}$$

for all ϕ except, possibly, at points on the boundary between regions with different properties. However, we need not concern ourselves with such boundary points; we are only interested in solutions to the scalar wave equation at interior points of homogeneous regions. Condition (4.6) then requires m to be an integer or zero; positive values of m are sufficient to generate all the linearly independent solutions to (4.3).

The solutions to (4.4) that are finite at $\theta = 0$ and $\theta = \pi$ are the *associated Legendre functions* of the first kind $P_n^m(\cos\theta)$ of degree n and order m, where $n = m, m + 1, \ldots$ (see, e.g., Courant and Hilbert, 1953, pp. 326, 327). These functions are orthogonal:

$$\int_{-1}^{1} P_n^m(\mu) P_{n'}^m(\mu)\, d\mu = \delta_{n'n} \frac{2}{2n+1} \frac{(n+m)!}{(n-m)!}, \tag{4.7}$$

where $\mu = \cos\theta$ and $\delta_{n'n}$, the Kronecker delta, is unity if $n = n'$ and zero otherwise. When $m = 0$ the associated Legendre functions are the *Legendre polynomials*, which are denoted by P_n.

If we introduce the dimensionless variable $\rho = kr$ and define the function $Z = R\sqrt{\rho}$, (4.5) becomes

$$\rho \frac{d}{d\rho}\left(\rho \frac{dZ}{d\rho}\right) + \left[\rho^2 - \left(n + \tfrac{1}{2}\right)^2\right] Z = 0. \tag{4.8}$$

The linearly independent solutions to (4.8) are the *Bessel functions* of first and second kind J_ν and Y_ν (the symbol N_ν is often used instead of Y_ν), where the *order* $\nu = n + \frac{1}{2}$ is half-integral. Therefore, the linearly independent solutions to (4.5) are the *spherical Bessel functions*

$$j_n(\rho) = \sqrt{\frac{\pi}{2\rho}}\, J_{n+1/2}(\rho), \tag{4.9}$$

$$y_n(\rho) = \sqrt{\frac{\pi}{2\rho}}\, Y_{n+1/2}(\rho), \tag{4.10}$$

where the constant factor $\sqrt{\pi/2}$ is introduced for convenience. The spherical Bessel functions satisfy the recurrence relations

$$z_{n-1}(\rho) + z_{n+1}(\rho) = \frac{2n+1}{\rho} z_n(\rho), \tag{4.11}$$

$$(2n+1) \frac{d}{d\rho} z_n(\rho) = n z_{n-1}(\rho) - (n+1) z_{n+1}(\rho), \tag{4.12}$$

where z_n is either j_n or y_n. From the first two orders

$$j_0(\rho) = \frac{\sin\rho}{\rho}, \qquad j_1(\rho) = \frac{\sin\rho}{\rho^2} - \frac{\cos\rho}{\rho},$$

$$y_0(\rho) = -\frac{\cos\rho}{\rho}, \qquad y_1(\rho) = -\frac{\cos\rho}{\rho^2} - \frac{\sin\rho}{\rho},$$

higher-order functions can be generated by recurrence. Note that for all orders n, $y_n(\mathrm{k}r)$ becomes infinite as r approaches the origin. In Fig. 4.2 we show $j_n(x)$ and $y_n(x)(n = 0, 1, 2, 3)$ for real values of x, although the spherical Bessel functions are not restricted to real arguments.

Any linear combination of j_n and y_n is also a solution to (4.5). If the mood were to strike us, therefore, we could just as well take as fundamental solutions to (4.5) any two linearly independent combinations. Two such combinations deserve special attention, the *spherical Bessel functions of the third kind* (sometimes called spherical Hankel functions):

$$h_n^{(1)}(\rho) = j_n(\rho) + iy_n(\rho), \tag{4.13}$$

$$h_n^{(2)}(\rho) = j_n(\rho) - iy_n(\rho). \tag{4.14}$$

We hasten to add that we have introduced even more Bessel functions neither for "completeness" nor for the further aggrandizement of Friedrich Wilhelm Bessel (1784–1846), who, with a veritable zoo of functions to his credit, not to mention infinite series, a revered inequality, an interpolation scheme, and various other mathematical artifacts, needs no publicity; as we shall see, (4.13) and (4.14) will save some labor, a sufficient reason for admitting more functions into our larder.

We have now done enough work to construct generating functions that satisfy the scalar wave equation in spherical polar coordinates:

$$\psi_{emn} = \cos m\phi P_n^m(\cos\theta) z_n(\mathrm{k}r), \tag{4.15}$$

$$\psi_{omn} = \sin m\phi P_n^m(\cos\theta) z_n(\mathrm{k}r), \tag{4.16}$$

where z_n is any of the four spherical Bessel functions j_n, y_n, $h_n^{(1)}$, or $h_n^{(2)}$. Moreover, because of the *completeness* of the functions $\cos m\phi, \sin m\phi$, $P_n^m(\cos\theta)$, $z_n(\mathrm{k}r)$, any function that satisfies the scalar wave equation in spherical polar coordinates may be expanded as an infinite series in the functions (4.15) and (4.16). The vector spherical harmonics generated by ψ_{emn} and ψ_{omn} are

$$\mathbf{M}_{emn} = \nabla \times (\mathbf{r}\psi_{emn}), \qquad \mathbf{M}_{omn} = \nabla \times (\mathbf{r}\psi_{omn}),$$

$$\mathbf{N}_{emn} = \frac{\nabla \times \mathbf{M}_{emn}}{\mathrm{k}}, \qquad \mathbf{N}_{omn} = \frac{\nabla \times \mathbf{M}_{omn}}{\mathrm{k}},$$

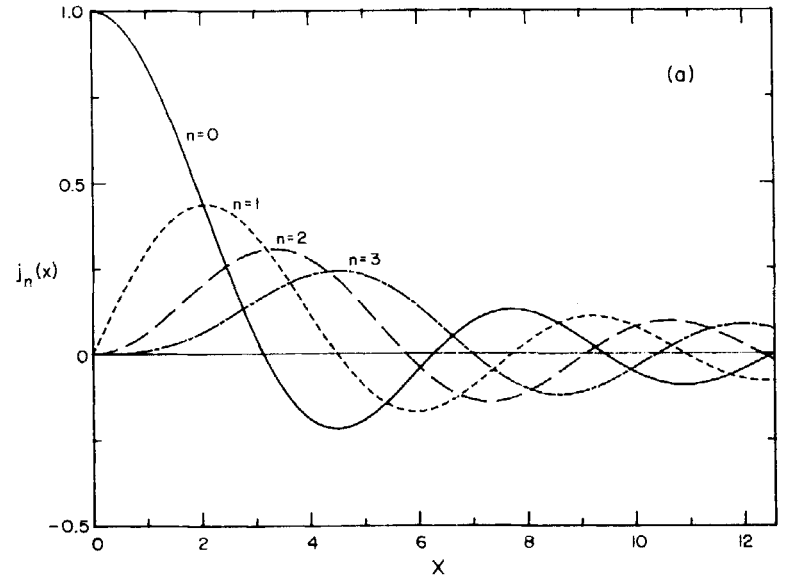

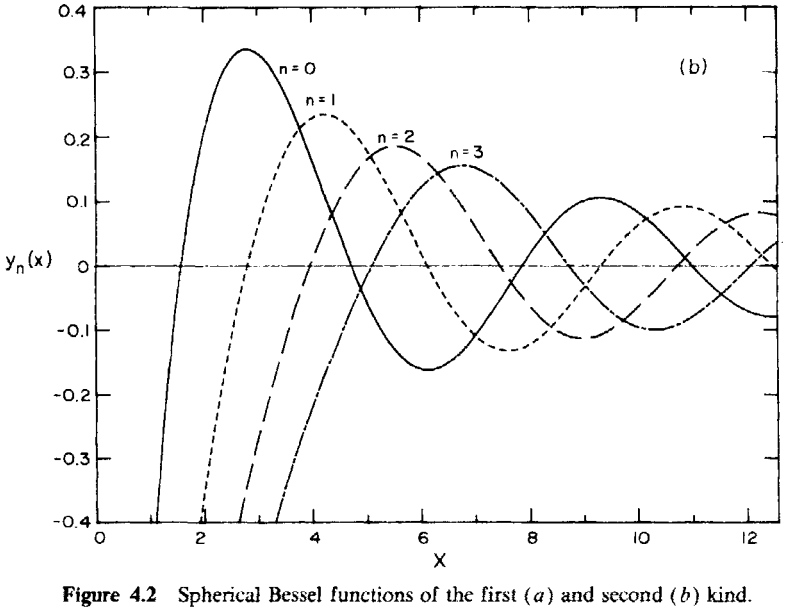

Figure 4.2 Spherical Bessel functions of the first (*a*) and second (*b*) kind.

which, in component form, may be written

$$\mathbf{M}_{emn} = \frac{-m}{\sin\theta}\sin m\phi\, P_n^m(\cos\theta) z_n(\rho)\hat{\mathbf{e}}_\theta - \cos m\phi \frac{dP_n^m(\cos\theta)}{d\theta} z_n(\rho)\hat{\mathbf{e}}_\phi, \tag{4.17}$$

$$\mathbf{M}_{omn} = \frac{m}{\sin\theta}\cos m\phi\, P_n^m(\cos\theta) z_n(\rho)\hat{\mathbf{e}}_\theta - \sin m\phi \frac{dP_n^m(\cos\theta)}{d\theta} z_n(\rho)\hat{\mathbf{e}}_\phi, \tag{4.18}$$

$$\mathbf{N}_{emn} = \frac{z_n(\rho)}{\rho}\cos m\phi\, n(n+1) P_n^m(\cos\theta)\hat{\mathbf{e}}_r + \cos m\phi \frac{dP_n^m(\cos\theta)}{d\theta}\frac{1}{\rho}\frac{d}{d\rho}[\rho z_n(\rho)]\hat{\mathbf{e}}_\theta - m\sin m\phi \frac{P_n^m(\cos\theta)}{\sin\theta}\frac{1}{\rho}\frac{d}{d\rho}[\rho z_n(\rho)]\hat{\mathbf{e}}_\phi, \tag{4.19}$$

$$\mathbf{N}_{omn} = \frac{z_n(\rho)}{\rho}\sin m\phi\, n(n+1) P_n^m(\cos\theta)\hat{\mathbf{e}}_r + \sin m\phi \frac{dP_n^m(\cos\theta)}{d\theta}\frac{1}{\rho}\frac{d}{d\rho}[\rho z_n(\rho)]\hat{\mathbf{e}}_\theta + m\cos m\phi \frac{P_n^m(\cos\theta)}{\sin\theta}\frac{1}{\rho}\frac{d}{d\rho}[\rho z_n(\rho)]\hat{\mathbf{e}}_\phi, \tag{4.20}$$

where the r-component of $\mathbf{N}_{mn}$ has been simplified by using the fact that P_n^m satisfies (4.4). Any solution to the field equations can now be expanded in an infinite series of the functions (4.17)–(4.20). Thus, armed with vector harmonics, we are ready to attack the problem of scattering by an arbitrary sphere.

4.2 EXPANSION OF A PLANE WAVE IN VECTOR SPHERICAL HARMONICS

Expansion of a plane wave in vector spherical harmonics is a lengthy, although straightforward, procedure. In this section we outline how one goes about determining the coefficients in such an expansion.

The problem with which we are concerned is scattering of a plane x-polarized wave, written in spherical polar coordinates as

$$\mathbf{E}_i = E_0 e^{ikr\cos\theta}\hat{\mathbf{e}}_x, \tag{4.21}$$

where

$$\hat{\mathbf{e}}_x = \sin\theta\cos\phi\hat{\mathbf{e}}_r + \cos\theta\cos\phi\hat{\mathbf{e}}_\theta - \sin\phi\hat{\mathbf{e}}_\phi, \tag{4.22}$$

by an arbitrary sphere. The first step toward the solution to this problem is

expanding (4.21) in vector spherical harmonics:

$$\mathbf{E}_i = \sum_{m=0}^{\infty} \sum_{n=m}^{\infty} (B_{emn}\mathbf{M}_{emn} + B_{omn}\mathbf{M}_{omn} + A_{emn}\mathbf{N}_{emn} + A_{omn}\mathbf{N}_{omn}). \tag{4.23}$$

Because $\sin m\phi$ is orthogonal to $\cos m'\phi$ for all m and m' it follows that $\mathbf{M}_{emn}$ and $\mathbf{M}_{omn}$ are orthogonal in the sense that

$$\int_0^{2\pi}\int_0^{\pi} \mathbf{M}_{em'n'} \cdot \mathbf{M}_{omn} \sin\theta \, d\theta \, d\phi = 0 \qquad (\text{all } m, m', n, n').$$

Similarly, $(\mathbf{N}_{omn}, \mathbf{N}_{emn})$, $(\mathbf{M}_{omn}, \mathbf{N}_{omn})$ and $(\mathbf{M}_{emn}, \mathbf{N}_{emn})$ are mutually orthogonal sets of functions. The orthogonality properties of $\cos m\phi$ and $\sin m\phi$ imply that all vector harmonics of different order m are mutually orthogonal.

To prove that the functions $(\mathbf{M}_{emn}, \mathbf{N}_{omn})$ and $(\mathbf{N}_{emn}, \mathbf{M}_{omn})$ are orthogonal, we must show that the integral

$$m\int_0^{\pi}\left(P_n^m \frac{dP_{n'}^m}{d\theta} + P_{n'}^m \frac{dP_n^m}{d\theta}\right) d\theta = P_n^m P_{n'}^m\Big|_0^{\pi} \tag{4.24}$$

vanishes for all n and n'. The associated Legendre function P_n^m is related to the mth derivative of the corresponding Legendre polynomial P_n,

$$P_n^m(\mu) = (1-\mu^2)^{m/2} \frac{d^m P_n(\mu)}{d\mu^m}, \tag{4.25}$$

where $\mu = \cos\theta$, from which it follows that P_n^m vanishes for $\theta = 0$ and $\theta = \pi$ except when $m = 0$. Therefore, (4.24) vanishes for all m, n, and n'.

The proof of the remaining orthogonality relations

$$\int_0^{2\pi}\int_0^{\pi} \mathbf{M}_{emn} \cdot \mathbf{M}_{emn'} \sin\theta \, d\theta \, d\phi = \int_0^{2\pi}\int_0^{\pi} \mathbf{M}_{omn} \cdot \mathbf{M}_{omn'} \sin\theta \, d\theta \, d\phi = 0,$$

$$\int_0^{2\pi}\int_0^{\pi} \mathbf{N}_{emn} \cdot \mathbf{N}_{emn'} \sin\theta \, d\theta \, d\phi = \int_0^{2\pi}\int_0^{\pi} \mathbf{N}_{omn} \cdot \mathbf{N}_{omn'} \sin\theta \, d\theta \, d\phi = 0,$$

when $n \neq n'$ and $m \neq 0$, requires showing that

$$\int_0^{\pi}\left(\frac{dP_n^m}{d\theta}\frac{dP_{n'}^m}{d\theta} + m^2 \frac{P_n^m P_{n'}^m}{\sin^2\theta}\right)\sin\theta \, d\theta = 0. \tag{4.26}$$

Because both P_n^m and $P_{n'}^m$ satisfy (4.4), we have, after a bit of manipulation

$$2\sin\theta\left(\frac{dP_n^m}{d\theta}\frac{dP_{n'}^m}{d\theta} + m^2\frac{P_n^m P_{n'}^m}{\sin^2\theta}\right) = \{n(n+1) + n'(n'+1)\}P_n^m P_{n'}^m \sin\theta + \frac{d}{d\theta}\left(\sin\theta \frac{dP_{n'}^m}{d\theta} P_n^m + \sin\theta \frac{dP_n^m}{d\theta} P_{n'}^m\right), \tag{4.27}$$

from which, together with the orthogonality relations for the P_n^m, (4.26) readily follows. When $m = 0$, $\mathbf{N}_{omn}$ and $\mathbf{M}_{omn}$ vanish; the orthogonality of the $\mathbf{M}_{emn}$ and the $\mathbf{N}_{emn}$ when $m = 0$ also follows from (4.26) and (4.27).

The orthogonality of all the vector spherical harmonics, which was established in the preceding section, implies that the coefficients in the expansion (4.23) are of the form

$$B_{emn} = \frac{\int_0^{2\pi}\int_0^{\pi} \mathbf{E}_i \cdot \mathbf{M}_{emn} \sin\theta \, d\theta \, d\phi}{\int_0^{2\pi}\int_0^{\pi} |\mathbf{M}_{emn}|^2 \sin\theta \, d\theta \, d\phi},$$

with similar expressions for B_{omn}, A_{emn}, and A_{omn}. It follows from (4.17), (4.20), and (4.22), together with the orthogonality of the sine and cosine, that $B_{emn} = A_{omn} = 0$ for all m and n. Moreover, the remaining coefficients vanish unless $m = 1$ for the same reason. The incident field is finite at the origin, which requires that $j_n(kr)$ is the appropriate spherical Bessel function in the generating functions ψ_{oln} and ψ_{eln}; we reject y_n because of its misbehavior at the origin. We shall append the superscript (1) to vector spherical harmonics for which the radial dependence of the generating functions is specified by j_n. Thus, the expansion for $\mathbf{E}_i$ has the form

$$\mathbf{E}_i = \sum_{n=1}^{\infty} \left(B_{oln}\mathbf{M}_{oln}^{(1)} + A_{eln}\mathbf{N}_{eln}^{(1)} \right). \tag{4.28}$$

The integral in the denominator of the expression for B_{oln} can readily be evaluated from (4.27); the numerator, however, contains the integral

$$\int_0^{\pi} \frac{d}{d\theta}\left(\sin\theta P_n^1\right) e^{i\rho\cos\theta} \, d\theta. \tag{4.29}$$

From (4.25) we have

$$P_n^1 = -\frac{dP_n}{d\theta}, \tag{4.30}$$

where the Legendre polynomials of degree n satisfy (4.4):

$$\frac{d}{d\theta}\left(\sin\theta \frac{dP_n}{d\theta}\right) = -n(n+1)P_n \sin\theta. \tag{4.31}$$

Thus, (4.29) is proportional to

$$\int_0^{\pi} e^{i\rho\cos\theta} P_n \sin\theta \, d\theta.$$

The final step is Gegenbauer's generalization of Poisson's integral (Watson,

1958, p. 50):

$$j_n(\rho) = \frac{i^{-n}}{2} \int_0^\pi e^{i\rho\cos\theta} P_n \sin\theta \, d\theta. \tag{4.32}$$

Without further fanfare, therefore, we arrive at the expansion coefficients

$$B_{oln} = i^n E_0 \frac{2n+1}{n(n+1)}. \tag{4.33}$$

The expansion coefficients A_{emn} are somewhat less tractable. For example, we are faced with the integral

$$\int_0^\pi P_n^1 \sin\theta e^{i\rho\cos\theta} \sin\theta \, d\theta, \tag{4.34}$$

which may be integrated by parts to yield

$$\frac{2n(n+1) j_n(\rho) i^n}{i\rho},$$

where we have also used (4.30), (4.31), and (4.32). The nastiest integral of the lot, however, is

$$\int_0^\pi \left(\cos\theta \frac{dP_n^1}{d\theta} + \frac{P_n^1}{\sin\theta} \right) e^{i\rho\cos\theta} \sin\theta \, d\theta, \tag{4.35}$$

which may be brought to earth by first multiplying (4.32) by ρ and then differentiating the resulting expression with respect to ρ. After a good bit of algebra we obtain

$$\frac{2n(n+1)i^n}{i\rho} \frac{d}{d\rho}(\rho j_n)$$

for (4.35). The expansion coefficients then follow straightforwardly:

$$A_{eln} = -iE_0 i^n \frac{2n+1}{n(n+1)}. \tag{4.36}$$

The desired expansion of a plane wave in spherical harmonics

$$\mathbf{E}_i = E_0 \sum_{n=1}^{\infty} i^n \frac{2n+1}{n(n+1)} \left(\mathbf{M}_{oln}^{(1)} - i\mathbf{N}_{eln}^{(1)} \right) \tag{4.37}$$

was not achieved without difficulty. This is undoubtedly the result of the unwillingness of a plane wave to wear a guise in which it feels uncomfortable; expanding a plane wave in spherical wave functions is somewhat like trying to force a square peg into a round hole. However, the reader who has painstak-

ingly followed the derivation of (4.37), and thereby acquired virtue through suffering, may derive some comfort from the knowledge that it is relatively clear sailing from here on.

4.3 THE INTERNAL AND SCATTERED FIELDS

Suppose that a plane x-polarized wave is incident on a homogeneous, isotropic sphere of radius a (Fig. 4.1). As we showed in the preceding section, the incident electric field may be expanded in an infinite series of vector spherical harmonics. The corresponding incident magnetic field is obtained from the curl of (4.37):

$$\mathbf{H}_i = \frac{-\mathrm{k}}{\omega\mu} E_o \sum_{n=1}^{\infty} i^n \frac{2n+1}{n(n+1)} \left(\mathbf{M}_{e1n}^{(1)} + i\mathbf{N}_{o1n}^{(1)}\right). \tag{4.38}$$

We may also expand the scattered electromagnetic field $(\mathbf{E}_s, \mathbf{H}_s)$ and the field $(\mathbf{E}_1, \mathbf{H}_1)$ inside the sphere in vector spherical harmonics. At the boundary between the sphere and the surrounding medium we impose the conditions (3.7):

$$(\mathbf{E}_i + \mathbf{E}_s - \mathbf{E}_1) \times \hat{\mathbf{e}}_r = (\mathbf{H}_i + \mathbf{H}_s - \mathbf{H}_1) \times \hat{\mathbf{e}}_r = 0. \tag{4.39}$$

The boundary conditions (4.39), the orthogonality of the vector harmonics, and the form of the expansion of the incident field dictate the form of the expansions for the scattered field and the field inside the sphere: the coefficients in these expansions vanish for all $m \neq 1$. Finiteness at the origin requires that we take $j_n(\mathrm{k}_1 r)$, where k_1 is the wave number in the sphere, as the appropriate spherical Bessel functions in the generating functions for the vector harmonics inside the sphere. Thus, the expansion of the field $(\mathbf{E}_1, \mathbf{H}_1)$ is

$$\begin{aligned} \mathbf{E}_1 &= \sum_{n=1}^{\infty} E_n \left(c_n \mathbf{M}_{o1n}^{(1)} - i d_n \mathbf{N}_{e1n}^{(1)}\right), \\ \mathbf{H}_1 &= \frac{-\mathrm{k}_1}{\omega\mu_1} \sum_{n=1}^{\infty} E_n \left(d_n \mathbf{M}_{e1n}^{(1)} + i c_n \mathbf{N}_{o1n}^{(1)}\right), \end{aligned} \tag{4.40}$$

where $E_n = i^n E_0 (2n+1)/n(n+1)$ and μ_1 is the permeability of the sphere.

In the region outside the sphere j_n and y_n are well behaved; therefore, the expansion of the scattered field involves both of these functions. However, it is convenient if we now switch our allegiance to the spherical Hankel functions $h_n^{(1)}$ and $h_n^{(2)}$. We can show that only one of these functions is required by considering the asymptotic expansions of the Hankel functions of order ν for large values of $|\rho|$ (Watson, 1958, p. 198):

$$\begin{aligned} H_\nu^{(1)}(\rho) &\sim \sqrt{\frac{2}{\pi\rho}}\, e^{i[\rho - \nu\pi/2 - \pi/4]} \sum_{m=0}^{\infty} \frac{(-1)^m (\nu, m)}{(2i\rho)^m}, \\ H_\nu^{(2)}(\rho) &\sim \sqrt{\frac{2}{\pi\rho}}\, e^{-i[\rho - \nu\pi/2 - \pi/4]} \sum_{m=0}^{\infty} \frac{(\nu, m)}{(2i\rho)^m}, \end{aligned} \tag{4.41}$$

where $(\nu, m) = \Gamma(\nu + m + 1/2)/m!\Gamma(\nu - m + 1/2)$ and Γ is the gamma function; $\Gamma(n + 1) = n!$ if n is a nonnegative integer. It follows from (4.41) that the spherical Hankel functions are asymptotically given by

$$h_n^{(1)}(\mathrm{k}r) \sim \frac{(-i)^n e^{i\mathrm{k}r}}{i\mathrm{k}r}, \qquad \mathrm{k}r \gg n^2 \tag{4.42}$$

$$h_n^{(2)}(\mathrm{k}r) \sim -\frac{i^n e^{-i\mathrm{k}r}}{i\mathrm{k}r}. \tag{4.43}$$

The first of these asymptotic expressions corresponds to an *outgoing* spherical wave; the second corresponds to an *incoming* spherical wave. If, on physical grounds, the scattered field is to be an outgoing wave at large distances from the particle, then only $h_n^{(1)}$ should be used in the generating functions. When we consider the scattered field at large distances we shall also need the asymptotic expression for the derivative of $h_n^{(1)}$; it follows from the identity

$$\frac{d}{d\rho} z_n = \frac{n z_{n-1} - (n + 1) z_{n+1}}{2n + 1}$$

and (4.42) that

$$\frac{dh_n^{(1)}}{d\rho} \sim \frac{(-i)^n e^{i\rho}}{\rho} \qquad (\rho \gg n^2). \tag{4.44}$$

The expansion of the scattered field is therefore

$$\begin{aligned} \mathbf{E}_s &= \sum_{n=1}^{\infty} E_n \left(i a_n \mathbf{N}_{e1n}^{(3)} - b_n \mathbf{M}_{o1n}^{(3)} \right), \\ \mathbf{H}_s &= \frac{\mathrm{k}}{\omega\mu} \sum_{n=1}^{\infty} E_n \left(i b_n \mathbf{N}_{o1n}^{(3)} + a_n \mathbf{M}_{e1n}^{(3)} \right), \end{aligned} \tag{4.45}$$

where we append the superscript (3) to vector spherical harmonics for which the radial dependence of the generating functions is specified by $h_n^{(1)}$.

4.3.1 Angle-Dependent Functions

It is now convenient to define the functions

$$\pi_n = \frac{P_n^1}{\sin\theta}, \qquad \tau_n = \frac{dP_n^1}{d\theta}. \tag{4.46}$$

The angle-dependent functions π_n and τ_n appear to pose no particular computational problems—at least no one has complained about their misbehavior in

print—and can be computed by upward recurrence from the relations

$$\pi_n = \frac{2n-1}{n-1}\mu\pi_{n-1} - \frac{n}{n-1}\pi_{n-2},$$
$$\tau_n = n\mu\pi_n - (n+1)\pi_{n-1}, \tag{4.47}$$

where $\mu = \cos\theta$, beginning with $\pi_0 = 0$ and $\pi_1 = 1$; π_n and τ_n are alternately even and odd functions of μ:

$$\pi_n(-\mu) = (-1)^{n-1}\pi_n(\mu), \qquad \tau_n(-\mu) = (-1)^n\tau_n(\mu). \tag{4.48}$$

Although π_n and τ_n are neither mutually orthogonal nor orthogonal to each other, it follows from (4.26) and (4.24) that $\pi_n + \tau_n$, as well as $\pi_n - \tau_n$, are orthogonal sets of functions:

$$\int_0^\pi (\tau_n + \pi_n)(\tau_m + \pi_m)\sin\theta\, d\theta = \int_0^\pi (\tau_n - \pi_n)(\tau_m - \pi_m)\sin\theta\, d\theta = 0$$
$$(m \neq n). \tag{4.49}$$

We can now write the vector spherical harmonics (4.17)–(4.20) (with $m = 1$) in the expansions of the internal field(4.40) and the scattered field (4.45) in a more concise form:

$$\mathbf{M}_{o1n} = \cos\phi\,\pi_n(\cos\theta)z_n(\rho)\hat{\mathbf{e}}_\theta - \sin\phi\,\tau_n(\cos\theta)z_n(\rho)\hat{\mathbf{e}}_\phi,$$

$$\mathbf{M}_{e1n} = -\sin\phi\,\pi_n(\cos\theta)z_n(\rho)\hat{\mathbf{e}}_\theta - \cos\phi\,\tau_n(\cos\theta)z_n(\rho)\hat{\mathbf{e}}_\phi,$$

$$\mathbf{N}_{o1n} = \sin\phi\, n(n+1)\sin\theta\,\pi_n(\cos\theta)\frac{z_n(\rho)}{\rho}\hat{\mathbf{e}}_r$$
$$+\sin\phi\,\tau_n(\cos\theta)\frac{[\rho z_n(\rho)]'}{\rho}\hat{\mathbf{e}}_\theta + \cos\phi\,\pi_n(\cos\theta)\frac{[\rho z_n(\rho)]'}{\rho}\hat{\mathbf{e}}_\phi$$

$$\mathbf{N}_{e1n} = \cos\phi\, n(n+1)\sin\theta\,\pi_n(\cos\theta)\frac{z_n(\rho)}{\rho}\hat{\mathbf{e}}_r$$
$$+\cos\phi\,\tau_n(\cos\theta)\frac{[\rho z_n(\rho)]'}{\rho}\hat{\mathbf{e}}_\theta - \sin\phi\,\pi_n(\cos\theta)\frac{[\rho z_n(\rho)]'}{\rho}\hat{\mathbf{e}}_\phi. \tag{4.50}$$

Superscripts will be appended to the functions **M** and **N** to denote the kind of spherical Bessel function z_n: (1) denotes $j_n(k_1 r)$ and (3) denotes $h_n^{(1)}(kr)$. As

noted previously, **M** has no radial component, and for sufficiently large kr the radial component of **N** for the scattered field is negligible compared with the transverse component.

We have shown in Fig. 4.2 how the functions j_n and y_n behave, and the functions $\sin\phi$, $\cos\phi$ are well known. Thus, it only remains for us to show the behavior of the functions π_n and τ_n, which determine the θ dependence of the fields. Polar plots of π_n and τ_n for $n = 1$–5 are shown in Fig. 4.3; these plots are more pleasing to the eye if we allow θ to range from 0 to 360°. Note

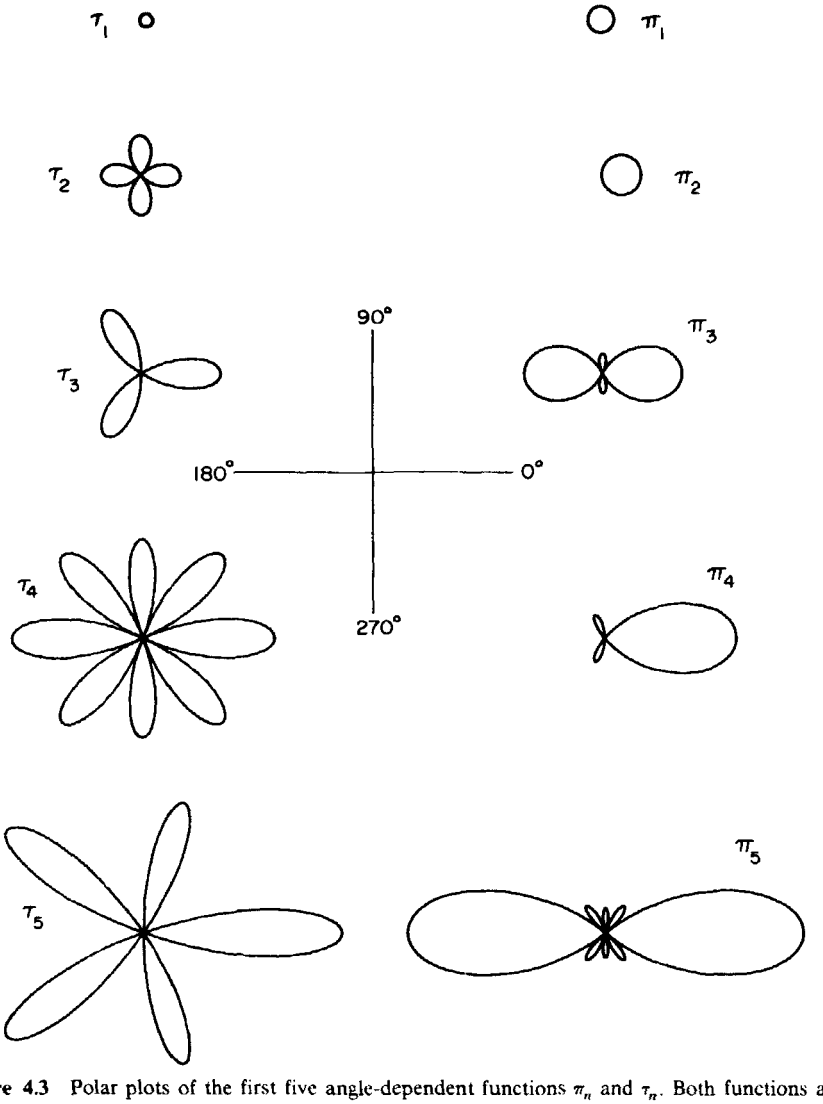

Figure 4.3 Polar plots of the first five angle-dependent functions π_n and τ_n. Both functions are plotted to the same scale.

that these functions (except π_1, which is constant) take on both positive and negative values; for example, τ_2 is positive from 0 to 45°, negative from 45 to 135°, and positive from 135 to 180°. As n increases, the number of lobes increases, with the result that the forward-directed lobe becomes narrower (i.e., the first zero occurs at smaller angles). The absence of a back-directed lobe in the polar plots of π_n and τ_n indicates that they are negative for backward directions; for example, τ_3 is negative for θ between about 149 and 180°. All the functions have forward-directed lobes (i.e., are positive in the forward direction), but the backward lobes disappear for alternate values of n. As we shall see, the larger the sphere, the more high-order functions π_n and τ_n are incorporated in the scattering diagram. Because of the behavior of these functions, therefore, the larger the sphere, the more heavily forward scattering directions are weighted compared with backscattering directions (alternate values of π_n or τ_n tend to cancel in backscattering directions), and the narrower the forward scattered peak.

4.3.2 Field Patterns: Normal Modes

The scattered electromagnetic field has been written as an infinite series in the vector spherical harmonics $\mathbf{M}_n$ and $\mathbf{N}_n$, the electromagnetic *normal modes* of the spherical particle. In the following section we shall discuss the conditions under which a single normal mode might be excited; in general, however, the scattered field is a superposition of normal modes, each weighted by the appropriate coefficient a_n or b_n. Diagrams from Mie's 1908 paper, which show the electric field lines corresponding to the transverse components of the first four normal modes, are given in Fig. 4.4. These diagrams have been reproduced in, among other places, Stratton (1941, p. 567), where so little discussion is given that they are easily misinterpreted, and in Tricker (1970, p. 226), where an excellent discussion of them is found. The field lines are shown on the surface of an imaginary sphere concentric with, but at a distance from, the particle. For each n there are two distinct types of modes: one for which there is no radial magnetic field component, called *transverse magnetic modes*, and another for which there is no radial electric field component, called *transverse electric modes*. As an aid in translating the confusing terminology often found for these modes, we have included in Fig. 4.4 other terms sometimes used, such as *electric type* or *E-waves* for the transverse magnetic modes, and *magnetic type* or *H-waves* for the transverse electric modes. Below each diagram we indicate the corresponding vector spherical harmonic together with the appropriate scattering coefficient. Although we have shown only the electric field patterns, the magnetic field patterns are readily obtained by rotation through an azimuthal angle of 90°; this follows from the relations [see (4.50)]

$$\mathbf{M}_{o1n}(\phi + \tfrac{1}{2}\pi) = \mathbf{M}_{e1n}(\phi); \qquad \mathbf{N}_{o1n}(\phi + \tfrac{1}{2}\pi) = \mathbf{N}_{e1n}(\phi)$$

and the expansions (4.45).

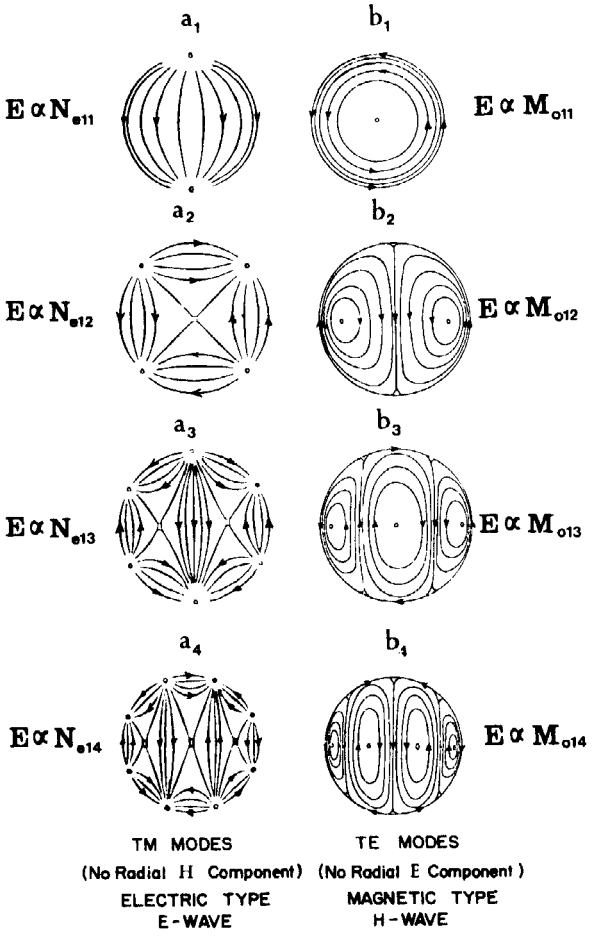

Figure 4.4 Electric field patterns: normal modes (Mie, 1908).

At first glance it may be confusing to see what appear to be free charges outside the particle, that is, points where the field lines appear to converge toward or diverge from. There clearly should be no free charges because each diagram represents field lines on the surface of an imaginary sphere in the medium surrounding the particle, which we may take to be free space. These apparent charge points are positions on the imaginary sphere at which the transverse field vanishes, and radial fields cannot be represented on a spherical surface. This can be made clearer by considering the radial component of the field for a particular mode. We have chosen the a_1 mode, which has particular importance later in the book; this is the field radiated by an oscillating electric dipole. Therefore, we can refer to the dipole radiation pattern for insight into the patterns shown in Fig. 4.4. Field lines in the xy plane ($\theta = \pi/2$) corre-

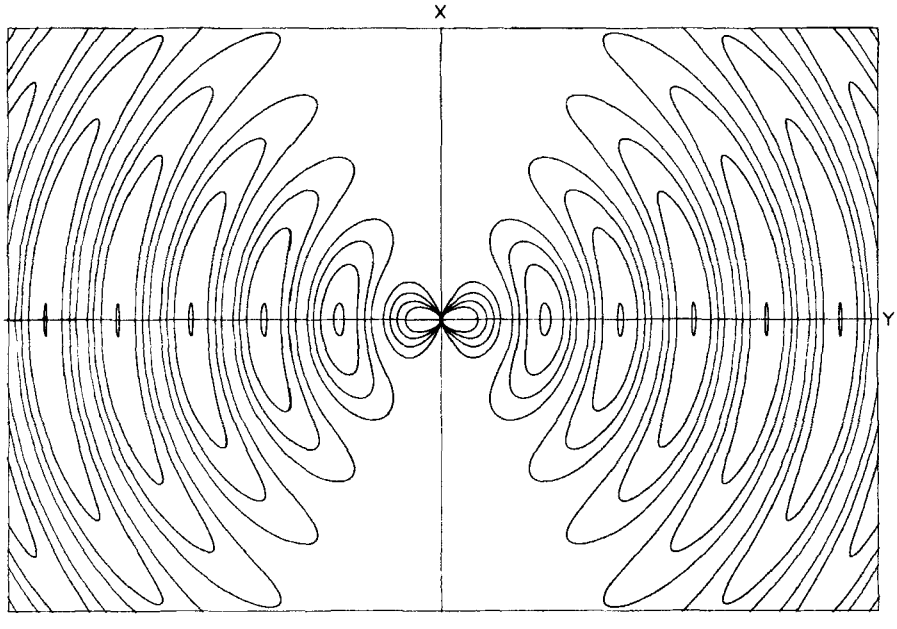

Figure 4.5 Field of a radiating dipole.

sponding to $i\mathbf{N}_{e11}^{(3)}$ are shown in Fig. 4.5. Note that, for a given distance r, the ϕ component of the field vanishes as we approach the x axis; along this axis the field is entirely radial. This, therefore, is why the field lines of the a_1 diagram in Fig. 4.4 vanish near the poles. Similar effects occur in each of the more complicated diagrams of Fig. 4.4.

4.3.3 Scattering Coefficients

We have arrived at the point where further understanding of scattering and absorption by a sphere is difficult to acquire without some numerical examples. What is needed now is some flesh to cover the dry bones of the formal theory; we should like to know how the various observable quantities vary with the size and optical properties of the sphere and the nature of the surrounding medium. To do so the first step is to obtain explicit expressions for the *scattering coefficients* a_n and b_n.

For a given n there are four unknown coefficients a_n, b_n, c_n, and d_n; thus, we need four independent equations, which are obtained from the boundary conditions (4.39) in component form:

$$\begin{aligned} E_{i\theta} + E_{s\theta} &= E_{1\theta}, \qquad E_{i\phi} + E_{s\phi} = E_{1\phi}, \\ H_{i\theta} + H_{s\theta} &= H_{1\theta}, \qquad H_{i\phi} + H_{s\phi} = H_{1\phi}, \end{aligned} \qquad r = a.$$

From the orthogonality of $\sin\phi$ and $\cos\phi$, the relations (4.49), the boundary conditions above, together with the expansions (4.37), (4.38), (4.40), (4.45), and the expressions (4.50) for the vector harmonics, we eventually obtain four linear equations in the expansion coefficients:

$$\begin{aligned} j_n(mx)c_n + h_n^{(1)}(x)b_n &= j_n(x), \\ \mu[mxj_n(mx)]'c_n + \mu_1[xh_n^{(1)}(x)]'b_n &= \mu_1[xj_n(x)]', \\ \mu m j_n(mx)d_n + \mu_1 h_n^{(1)}(x)a_n &= \mu_1 j_n(x), \\ [mxj_n(mx)]'d_n + m[xh_n^{(1)}(x)]'a_n &= m[xj_n(x)]', \end{aligned} \tag{4.51}$$

where the prime indicates differentiation with respect to the argument in parentheses and the *size parameter* x and the *relative refractive index* m are

$$x = \mathrm{k}a = \frac{2\pi Na}{\lambda}, \qquad m = \frac{\mathrm{k}_1}{\mathrm{k}} = \frac{N_1}{N}.$$

N_1 and N are the refractive indices of particle and medium, respectively. The four simultaneous linear equations (4.51) are easily solved for the coefficients of the field inside the particle

$$\begin{aligned} c_n &= \frac{\mu_1 j_n(x)[xh_n^{(1)}(x)]' - \mu_1 h_n^{(1)}(x)[xj_n(x)]'}{\mu_1 j_n(mx)[xh_n^{(1)}(x)]' - \mu h_n^{(1)}(x)[mxj_n(mx)]'}, \\ d_n &= \frac{\mu_1 m j_n(x)[xh_n^{(1)}(x)]' - \mu_1 m h_n^{(1)}(x)[xj_n(x)]'}{\mu m^2 j_n(mx)[xh_n^{(1)}(x)]' - \mu_1 h_n^{(1)}(x)[mxj_n(mx)]'}, \end{aligned} \tag{4.52}$$

and the scattering coefficients

$$\begin{aligned} a_n &= \frac{\mu m^2 j_n(mx)[xj_n(x)]' - \mu_1 j_n(x)[mxj_n(mx)]'}{\mu m^2 j_n(mx)[xh_n^{(1)}(x)]' - \mu_1 h_n^{(1)}(x)[mxj_n(mx)]'}, \\ b_n &= \frac{\mu_1 j_n(mx)[xj_n(x)]' - \mu j_n(x)[mxj_n(mx)]'}{\mu_1 j_n(mx)[xh_n^{(1)}(x)]' - \mu h_n^{(1)}(x)[mxj_n(mx)]'}, \end{aligned} \tag{4.53}$$

Note that the denominators of c_n and b_n are identical as are those of a_n and d_n. If for a particular n the frequency (or radius) is such that one of these denominators is very small, the corresponding normal mode will dominate the scattered field. The a_n mode is dominant if the condition

$$\frac{[xh_n^{(1)}(x)]'}{h_n^{(1)}(x)} = \frac{\mu_1[mxj_n(mx)]'}{\mu m^2 j_n(mx)}, \tag{4.54}$$

is approximately satisfied; similarly, the b_n mode is dominant if

$$\frac{[xh_n^{(1)}(x)]'}{h_n^{(1)}(x)} = \frac{\mu[mxj_n(mx)]'}{\mu_1 j_n(mx)} \tag{4.55}$$

is approximately satisfied. In general, of course, the scattered field is a superposition of normal modes.

The frequencies for which (4.54) and (4.55) are exactly satisfied, the so-called *natural* frequencies of the sphere (Stratton, 1941, p. 554), are *complex*, and the associated modes are sometimes said to be *virtual*. If the imaginary parts of these complex frequencies are small compared with the real parts, the latter correspond approximately to the real frequencies of incident electromagnetic waves which excite the various electromagnetic modes. Fuchs and Kliewer (1968) have thoroughly investigated the virtual modes of an ionic sphere with realistic frequency-dependent optical constants; they found that the modes fell naturally into three classes: low-frequency modes, high-frequency modes, and surface modes. In subsequent chapters we shall have more to say about electromagnetic modes in small particles, particularly in Chapter 12, where surface modes will be discussed at length.

The scattering coefficients (4.53) can be simplified somewhat by introducing the *Riccati–Bessel functions*:

$$\psi_n(\rho) = \rho j_n(\rho), \qquad \xi_n(\rho) = \rho h_n^{(1)}(\rho).$$

If we take the permeability of the particle and the surrounding medium to be the same, then

$$a_n = \frac{m\psi_n(mx)\psi_n'(x) - \psi_n(x)\psi_n'(mx)}{m\psi_n(mx)\xi_n'(x) - \xi_n(x)\psi_n'(mx)}, \tag{4.56}$$

$$b_n = \frac{\psi_n(mx)\psi_n'(x) - m\psi_n(x)\psi_n'(mx)}{\psi_n(mx)\xi_n'(x) - m\xi_n(x)\psi_n'(mx)}. \tag{4.57}$$

Note that a_n and b_n vanish as m approaches unity; this is as it should be: when the particle disappears, so does the scattered field.

As far as notation for the scattering coefficients is concerned, we have followed as much as possible van de Hulst (1957) and Kerker (1969), with the exception of the opposite sign convention for the time-harmonic factor $\exp(-i\omega t)$. Kerker (1969, p. 60) gives a table comparing the notation of various authors who have written on the theory of scattering by a sphere.

4.4 CROSS SECTIONS AND MATRIX ELEMENTS

Although we considered only scattering of x-polarized light in the preceding section, the scattered field for arbitrary linearly polarized incident light, and

hence any polarization state, follows from the symmetry of the particle. For example, the scattered electric fields for equal-amplitude incident x-polarized and y-polarized plane waves are related by

$$\mathbf{E}_s(\phi;\ x\text{-polarized}) = \mathbf{E}_s\left(\phi + \frac{\pi}{2};\ y\text{-polarized}\right).$$

Thus, if we have in hand the scattering coefficients a_n and b_n, we can determine all the measurable quantities associated with scattering and absorption, such as cross sections and scattering matrix elements.

4.4.1 Cross Sections

We could obtain cross sections for a sphere by appealing to the expressions for an arbitrary particle that were derived in Section 3.4 by calculating the net rate W_a at which electromagnetic energy crosses the surface of an imaginary sphere centered on the particle. If the surrounding medium is nonabsorbing, W_a is independent of the radius of this imaginary sphere, which for convenience was chosen to be sufficiently large that the far-field approximation for the electromagnetic field could be used. However, it is possible to derive expressions for the cross sections of a spherical particle exactly, something that seems to have been overlooked by previous authors. Therefore, it seems worthwhile to provide such a derivation. In so doing, we shall show some of the mathematical properties of the spherical Bessel functions; we may also acquire a bit more confidence in the optical theorem.

As before, we write W_a as $W_{\text{ext}} - W_s$, where

$$W_{\text{ext}} = \tfrac{1}{2}\,\text{Re}\int_0^{2\pi}\int_0^{\pi}\left(E_{i\phi}H_{s\theta}^* - E_{i\theta}H_{s\phi}^* - E_{s\theta}H_{i\phi}^* + E_{s\phi}H_{i\theta}^*\right)r^2\sin\theta\,d\theta\,d\phi,$$

$$W_s = \tfrac{1}{2}\,\text{Re}\int_0^{2\pi}\int_0^{\pi}\left(E_{s\theta}H_{s\phi}^* - E_{s\phi}H_{s\theta}^*\right)r^2\sin\theta\,d\theta\,d\phi, \tag{4.58}$$

and the radius $r \geq a$ of the imaginary sphere is arbitrary. On physical grounds we know that W_{ext} and W_s are independent of the polarization state of the incident light. Therefore, in evaluating the integrals (4.58) we may take the incident light to be x-polarized:

$$E_{i\theta} = \frac{\cos\phi}{\rho}\sum_{n=1}^{\infty} E_n(\psi_n\pi_n - i\psi_n'\tau_n), \qquad H_{i\theta} = \frac{\mathrm{k}}{\omega\mu}\tan\phi\,E_{i\theta},$$

$$E_{i\phi} = \frac{\sin\phi}{\rho}\sum_{n=1}^{\infty} E_n(i\psi_n'\pi_n - \psi_n\tau_n), \qquad H_{i\phi} = \frac{-\mathrm{k}}{\omega\mu}\cot\phi\,E_{i\phi},$$

where $\rho = kr$. The corresponding scattered field is

$$\begin{aligned} E_{s\theta} &= \frac{\cos\phi}{\rho} \sum_{n=1}^{\infty} E_n(ia_n\xi_n'\tau_n - b_n\xi_n\pi_n), \\ E_{s\phi} &= \frac{\sin\phi}{\rho} \sum_{n=1}^{\infty} E_n(b_n\xi_n\tau_n - ia_n\xi_n'\pi_n), \\ H_{s\theta} &= \frac{k}{\omega\mu} \frac{\sin\phi}{\rho} \sum_{n=1}^{\infty} E_n(ib_n\xi_n'\tau_n - a_n\xi_n\pi_n), \\ H_{s\phi} &= \frac{k}{\omega\mu} \frac{\cos\phi}{\rho} \sum_{n=1}^{\infty} E_n(ib_n\xi_n'\pi_n - a_n\xi_n\tau_n). \end{aligned} \tag{4.59}$$

If we assume that the series expansions (4.59) may be substituted in the integral for W_s and the resulting product series integrated term by term, we obtain

$$W_s = \frac{\pi|E_0|^2}{k\omega\mu} \sum_{n=1}^{\infty} (2n+1)\mathrm{Re}\{g_n\}(|a_n|^2 + |b_n|^2),$$

where we have used (4.24) and the relation

$$\int_0^{\pi} (\pi_n\pi_m + \tau_n\tau_m)\sin\theta\, d\theta = \delta_{nm} \frac{2n^2(n+1)^2}{2n+1},$$

which follows from (4.27). The quantity g_n, defined as $-i\xi_n^*\xi_n'$, may be written in the form

$$g_n = (\chi_n^*\psi_n' - \psi_n^*\chi_n') - i(\psi_n^*\psi_n' + \chi_n^*\chi_n'),$$

where the Riccati–Bessel function χ_n is $-\rho y_n(\rho)$ and, therefore, $\xi_n = \psi_n - i\chi_n$. The functions ψ_n and χ_n are real for real argument; therefore, if we use the Wronskian (Antosiewicz, 1964)

$$\chi_n\psi_n' - \psi_n\chi_n' = 1, \tag{4.60}$$

it follows that the scattering cross section is

$$C_{\mathrm{sca}} = \frac{W_s}{I_i} = \frac{2\pi}{k^2} \sum_{n=1}^{\infty} (2n+1)(|a_n|^2 + |b_n|^2). \tag{4.61}$$

Similarly, the extinction cross section is

$$C_{\mathrm{ext}} = \frac{W_{\mathrm{ext}}}{I_i} = \frac{2\pi}{k^2} \sum_{n=1}^{\infty} (2n+1)\mathrm{Re}\{a_n + b_n\}, \tag{4.62}$$

where, as in the derivation of the scattering cross section, the key step is the relation (4.60).

4.4.2 Examples of Extinction: Interference and Ripple Structure; Reddening

We now pause in the mathematical development to consider a few examples of extinction. A more complete discussion of extinction will be given in Chapter 11, which is devoted exclusively to this subject. The computational methods used to generate these examples will be discussed later in this chapter. For our brief look at extinction we have chosen water droplets in air; the wavelength-dependent optical constants—from radio to ultraviolet—that were used in these calculations are given in Chapter 10. Calculated extinction curves for three different radii are shown in Fig. 4.6, where extinction efficiency $Q_{ext} = C_{ext}/\pi a^2$ is plotted as a function of inverse wavelength $1/\lambda$. This somewhat unconventional method of displaying extinction may cause some readers to reel in horror, particularly when it is noted that the curves in Fig. 4.6 show marked deviations from those more commonly encountered; extinction efficiencies are usually shown as functions of x for a *fixed* refractive index m, a practice hallowed by tradition. Although the traditional method of displaying extinction is not necessarily incorrect, it is often misleading: x and m are *mathematically* independent variables but they may not be *physically* independent. This elementary fact is often lost sight of when x is considered to be merely a dimensionless variable that is indifferent to whether it changes because of varying wavelength or radius. For if the wavelength varies, so must m: no material substance has optical constants independent of wavelength except over a narrow range. Unfortunately, in some areas to which light scattering theory has been applied, full realization of this has only slowly dawned; the result has been spurious conclusions based on faulty reasoning. One of the central themes of this book is that full understanding of light scattering and absorption by particles requires understanding optical properties of bulk matter. The reason for the traditional method of displaying extinction has more to do with convenience than with fidelity to physical reality: it is relatively easy to calculate Q_{ext} as a function of x for fixed m. The curves shown in Fig. 4.6, however, require considerably more effort than is usual: at each of the many wavelengths for which computations are done, the correct optical properties must be used. The effort required to compute Q_{ext} *per se* is greatly overshadowed by that entailed in compiling optical constants from many sources and suitably interpolating between measured data points. The reward for this effort, however, is a more physically accurate picture of extinction.

In the region where water is weakly absorbing (between about 0.5 and 5 μm^{-1}) the extinction curve for a 1.0 μm droplet has several features: (1) a series of regularly spaced broad maxima and minima called the *interference structure*, which oscillates approximately about the value 2; (2) irregular fine

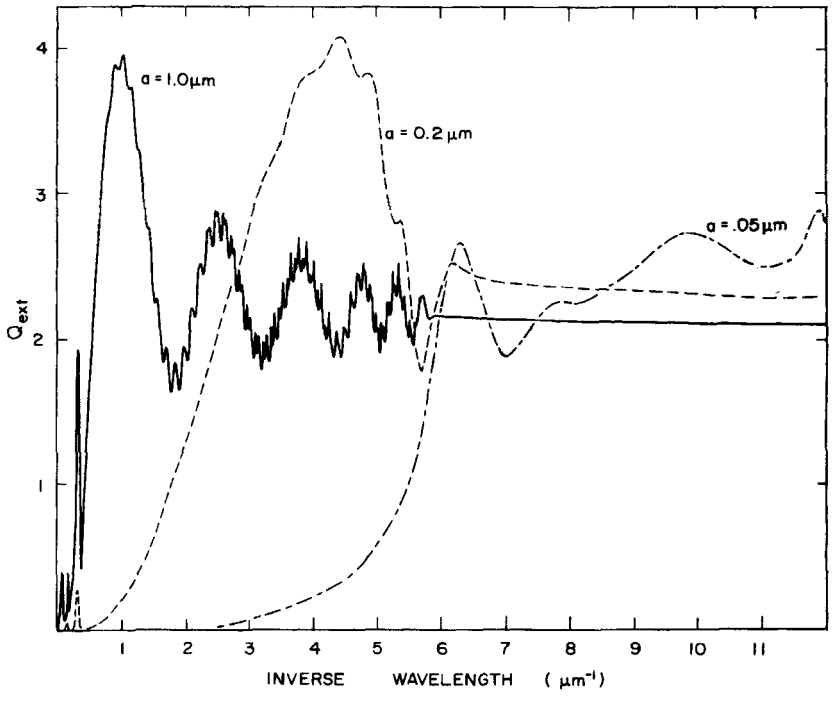

Figure 4.6 Extinction efficiencies for water droplets in air; plotting increment = 0.01 μm^{-1}.

structure called the *ripple structure*; and (3) monotonically increasing extinction with decreasing wavelength for $a < \lambda$. We shall briefly consider each of these in turn.

For large ($\gg n^2$)x and $|mx|$ the *numerator* of a_n is approximately

$$\frac{(m-1)\sin[x - n\pi/2]\cos[mx - n\pi/2] + m\sin[x(m-1)]}{x}. \tag{4.63}$$

To the same degree of approximation the numerator of b_n is

$$\frac{(1-m)\sin[x - n\pi/2]\cos[mx - n\pi/2] + \sin[x(m-1)]}{mx}. \tag{4.64}$$

To obtain (4.63) and (4.64) from (4.56) and (4.57) we used the asymptotic relation

$$\psi_n(\rho) \sim \sin(\rho - n\pi/2) \qquad (|\rho| \gg n^2). \tag{4.65}$$

Note that the numerator of both a_n and b_n contains the common term $\sin[x(m-1)]$, which is independent of n; thus, we expect the extinction cross

section maxima to be approximately determined by the maxima of this function, which occur for $x(m-1) = (2p+1)\pi/2$, where p is an integer. Therefore, the separation $\Delta(1/\lambda)$ between the maxima of $\sin[x(m-1)]$, over a wavelength region for which m is approximately constant and real, is $1/2a(m-1)$. For water at or near visible wavelengths, m may be taken to be about 1.33; thus, we expect the cross-section maxima for a 1.0-μm-radius droplet to be separated by about 1.5 μm^{-1}. That this is indeed so is apparent from Fig. 4.6. The origin of the term "interference structure" applied to these broad extinction peaks lies in the interpretation of extinction as interference between the incident and forward-scattered light (see Section 3.4). For if we adopt the viewpoint of elementary optics, the phase difference $\Delta\phi$ between a ray that traverses a large transparent sphere without deviation (i.e., the forward-scattered or central ray) and a ray that traverses the same physical path outside the sphere is

$$\Delta\phi = \frac{2\pi}{\lambda} 2a(N_1 - N) = 2x(m-1).$$

The condition for destructive interference between these two rays is $\Delta\phi = (2p+1)\pi$ or, equivalently, $x(m-1) = (2p+1)\pi/2$, which is the same condition as that obtained by examining the numerators of a_n and b_n.

We shall defer detailed discussion of the ripple structure, which is considerably more complicated both mathematically and physically than the interference structure, until Chapter 11. Suffice it to say for the moment that the ripple structure has its origins in the roots of the transcendental equations (4.54) and (4.55), the conditions under which the *denominators* of the scattering coefficients vanish.

Both the interference structure and the ripple structure are strongly damped when absorption becomes large, as it does in water if $1/\lambda$ is greater than about 6 μm^{-1}; this is analogous to damping of interference bands in the transmission spectrum of a slab (see Fig. 2.8). If the droplet is small compared with the wavelength, then peaks in the *bulk* absorption spectrum are seen in the *particle* extinction spectrum; for example, the extinction peaks in Fig. 4.6 at about 6 μm^{-1} for a 0.05-μm-radius droplet and at about 0.3 μm^{-1} for a 1.0-μm droplet are neither interference nor ripple structure but bulk absorption peaks. This illustrates the fact that absorption dominates over scattering for small a/λ if there is any appreciable bulk absorption.

A familiar phenomenon is *reddening* of white light on passing through a collection of very small particles. This can be demonstrated easily by putting a few drops of milk into a container of pure water: a collimated beam of white light takes on a reddish tint after transmission through this suspension because the shorter-wavelength blue light is extinguished more effectively than the longer-wavelength red light. Rising extinction toward shorter wavelengths is a general characteristic of nonabsorbing particles small compared with the wavelength; this is exhibited in the extinction curves in Fig. 4.6 for the two

smaller particles. Everyone is familiar with such effects through the beautiful red and orange hues of sunset skies, which are partly the result of molecular scattering. Small particles can enhance reddening of the sunset. Periods of strong volcanic activity have been known to increase the beauty of sunset colors for more than a year because of particles in the atmosphere; high levels of particulate air pollution tend to increase the sunset reddening.

Reddening because of extinction by small particles is certainly not limited to the terrestrial environment. Dust particles between stars extinguish blue light more efficiently than red light; starlight transmitted through this dust, therefore, is reddened. This effect is so reliable and uniform when averaged over many thousands of light years that it can be used to measure distances to stars in our galaxy. A "highly reddened star," as the jargon goes, is one that has a large quantity of interstellar dust between it and the observer. It is obvious from Fig. 4.6 that extinction is quite size dependent; for this reason, extinction has occasionally been used to size particles. In fact, this size dependence provides us with our best evidence that interstellar dust grains are predominantly submicron. In the laboratory, however, other types of measurements, such as angular scattering, are usually preferable for particle sizing.

Reddening occurs for collections of particles regardless of their size distribution provided that they are small compared with the wavelength. The opposite spectral effect, "bluing," can be seen on the high-frequency side of the extinction peaks in Fig. 4.6. Such bluing *is* highly dependent on the size distribution and tends to vanish, as do the other characteristics of the interference structure, as the dispersion of particle radii increases. Thus, bluing of sunlight by particles in the atmosphere is quite rare although not unheard of: it happens "once in a blue moon." This saying evidently originates from the fact that there have been a few times recorded in history when the sun and the moon were observed to be blue, such as after giant eruptions of the volcano Krakatoa and following huge forest fires in Canada. According to the conventional explanation, the conditions necessary for this anomalous extinction, which include a narrow range of particle sizes, are rarely met.

4.4.3 The Extinction Paradox; Scalar Diffraction Theory

We noted in the preceding section that Q_{ext} appears to approach the limiting value 2 as the size parameter increases:

$$\lim_{x \to \infty} Q_{\text{ext}}(x, m) = 2,$$

which is *twice* as large as that predicted by geometrical optics. Yet geometrical optics is considered to be a good approximation if all dimensions are much larger than the wavelength. Moreover, $Q_{\text{ext}} = 2$ contradicts "common sense": we do not expect a large object to remove twice the energy that is incident on it. This perhaps puzzling result is called the *extinction paradox*, which we shall try to resolve in the following paragraphs.

Although geometrical optics is a good approximation to the exact wave theory for large objects, no matter how large an object is it still has an *edge* in the neighborhood of which geometrical optics fails to be valid. Therefore, let us analyze extinction by a large sphere of radius a using a combination of geometrical optics and scalar diffraction theory.

The fundamental problem in scalar diffraction theory is to determine the value of a scalar wave ψ at a point P given the value of ψ and $\nabla\psi$ on a closed surface S surrounding P. A concise and lucid treatment of this theory is given by Wangsness (1963), who shows that

$$\psi(P) = \frac{1}{4\pi}\int_S \left\{ \frac{e^{ikR}}{R}\nabla\psi - \psi\nabla\left(\frac{e^{ikR}}{R}\right)\right\}\cdot\hat{\mathbf{n}}\, dA, \tag{4.66}$$

where R is the distance from P to a point on S and $\hat{\mathbf{n}}$ is the outward directed normal to S. Equation (4.66) is not restricted to electromagnetic waves but applies equally well to any scalar quantity that satisfies the wave equation $\nabla^2\psi + k^2\psi = 0$.

An amount of energy $I_i\pi a^2$ is removed from a beam with irradiance I_i as a result of reflection, refraction, and absorption of the rays that are incident on the sphere; that is, every ray is either absorbed or changes its direction and is therefore counted as having been removed from the incident beam. An *opaque disk* of radius a also removes an amount of energy $I_i\pi a^2$, and to the extent that scalar diffraction theory is valid, a sphere and an opaque disk have the same diffraction pattern. Therefore, for purposes of this analysis, we may replace the sphere by an opaque disk.

Although we shall be interested primarily in diffraction by an opaque circular disk, no extra labor is entailed if the shape of the planar obstacle is unrestricted at this stage of our argument (Fig. 4.7*a*). It is more convenient to consider diffraction by a planar *aperture*, with the same shape and dimensions as the obstacle, in an otherwise opaque screen (Fig. 4.7*b*). If $\psi(P)$ is the value of the wave function at P when the aperture is in place, we can invoke *Babinet's principle*,

$$\bar{\psi}(P) + \psi(P) = \psi_0(P), \tag{4.67}$$

to obtain the wave function $\bar{\psi}$ when the obstacle is in place, where ψ_0 is the unimpeded (incident) wave function, which we take to be a plane wave $E_0\exp(ikz)$.

To evaluate the integral in (4.66) we need to know ψ and its gradient over the surface S. It is physically plausible to assume that the only contribution to $\psi(P)$ comes from the aperture $\mathcal{A}$, over which ψ may be approximated by the incident wave function ψ_0. With this assumption (4.66) becomes

$$\psi(P) = \frac{-ikE_0}{4\pi}\int_{\mathcal{A}} \frac{e^{ikR}}{R}(1 - \hat{\mathbf{e}}_R\cdot\hat{\mathbf{e}}_z)\, dA, \tag{4.68}$$

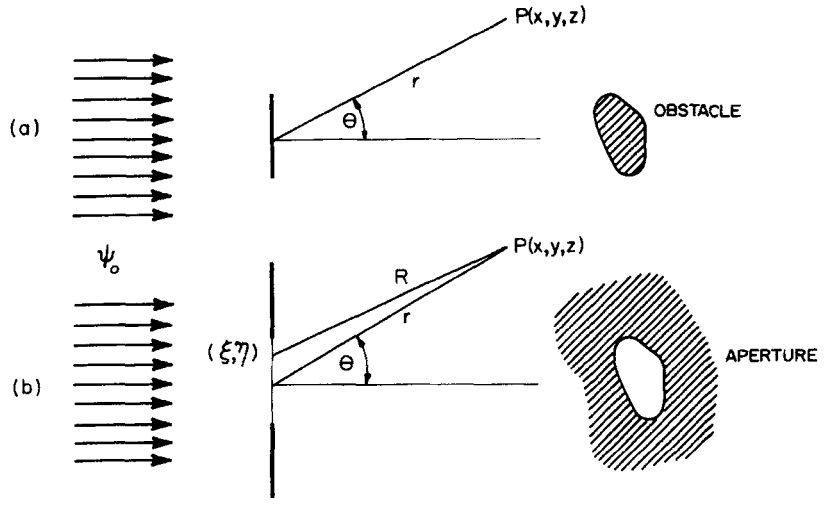

Figure 4.7 (*a*) Diffraction by an opaque planar obstacle. (*b*) Diffraction by an aperture with the same shape as the obstacle.

where we have also taken $kR \gg 1$; that is, the point P is at a distance from the aperture large compared with the wavelength. The unit vector $\hat{\mathbf{e}}_R$ is directed along the line from P to a point on the aperture with coordinates (ξ, η), and the distance R is

$$R = \sqrt{r^2 - 2x\xi - 2y\eta + \xi^2 + \eta^2}\,. \tag{4.69}$$

If the linear dimensions of the aperture are small compared with r, we can expand (4.69) in powers of ξ/r and η/r; *Fraunhofer diffraction* results if we terminate this expansion at linear terms:

$$\begin{aligned} \psi(P) &= E_0 \frac{e^{ikr}}{ikr} S(\theta, \phi), \\ S(\theta, \phi) &= \frac{k^2}{4\pi} \int_{\mathcal{A}} e^{-ik \sin\theta(\xi \cos\phi + \eta \sin\phi)} (1 + \cos\theta)\, d\xi\, d\eta. \end{aligned} \tag{4.70}$$

Therefore, with the obstacle in place, we have from (4.67) and (4.70),

$$\bar{\psi}(P) = E_0 e^{ikz} - E_0 \frac{e^{ikr}}{ikr} S(\theta, \phi). \tag{4.71}$$

The first term in (4.71) is just the incident wave; the second term is the wave scattered (diffracted) by the obstacle. The optical theorem for scalar waves is

formally identical to that for vector waves, (3.24); thus, the extinction cross section is

$$C_{\text{ext}} = \frac{4\pi}{k^2} \operatorname{Re}\{S(\theta = 0)\} = 2G, \tag{4.72}$$

where G is the area of the obstacle. Therefore, the extinction cross section of the obstacle is twice its geometrical cross section: all the energy incident on the opaque obstacle, an amount equal to $I_i G$, is absorbed; in addition, an equal amount of energy $W_s = I_i C_{\text{sca}}$, where

$$C_{\text{sca}} = \int_0^{2\pi} \int_0^{\pi} \frac{|S(\theta, \phi)|^2}{k^2} \sin\theta \, d\theta \, d\phi = G,$$

is scattered (diffracted) by the obstacle. Roughly speaking, we may say that the incident wave is influenced beyond the physical boundaries of the obstacle: the edge deflects rays in its neighborhood, rays that, from the viewpoint of geometrical optics, would have passed unimpeded. These rays, regardless of how small the angle through which they are deflected, are counted as having been removed from the incident beam and therefore contribute to the total extinction. To the extent that replacing a particle very much larger than the wavelength by an opaque planar obstacle with the same projected area is a valid approximation, the same interpretation elucidates why the extinction cross section of such a particle is twice its geometrical cross section.

We have yet to explain why $C_{\text{ext}} = 2G$ is not necessarily observed. To do so it will help if we consider a specific example. The scattering amplitude for a circular disk is independent of the azimuthal angle ϕ:

$$S(\theta) = \frac{k^2}{4\pi} \int_{\mathcal{A}} e^{-ik\xi \sin\theta} (1 + \cos\theta) \, d\xi \, d\eta. \tag{4.73}$$

We can evaluate the integral in (4.73) by transforming to plane polar coordinates and using the integral representation of the Bessel function J_0,

$$J_0(z) = \frac{1}{\pi} \int_0^{\pi} e^{iz\cos\psi} d\psi$$

together with the identity $d(zJ_1)/dz = zJ_0$; the result is

$$S(\theta) = x^2 \frac{(1 + \cos\theta)}{2} \frac{J_1(x \sin\theta)}{x \sin\theta}.$$

The size parameter is very large and $J_1(x \sin\theta)/x \sin\theta$ is negligibly small for $x \sin\theta$ greater than about 10; therefore, the factor $(1 + \cos\theta)/2$ is unity to a very good approximation over the angular region of interest. In Fig. 4.8 we show the scattering diagram normalized to the forward direction as a function of $x \sin\theta$. Note that almost all the scattered light is confined within a cone of

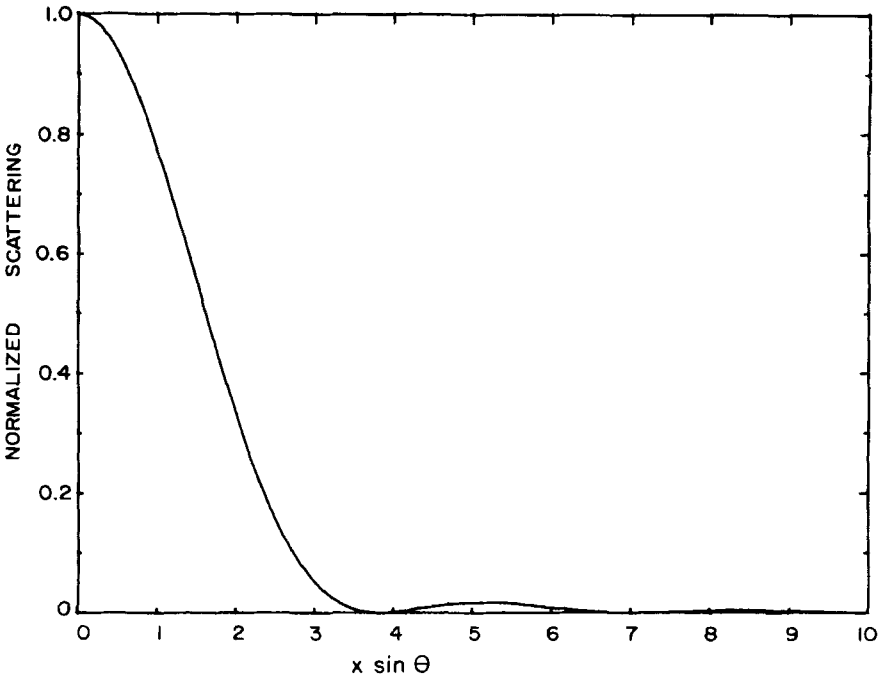

Figure 4.8 Scattering diagram for diffraction by a circular disk.

half-angle $\theta \simeq 10/x$. If a detector is to record the full extinction by a large spherical object, its acceptance angle must be much less than this, say $\theta_{acc} < 1/2x$. Thus, in any measurement of extinction by particles much larger than the wavelength, the possible effect of instrument geometry should be considered carefully. Failure to do so may result in spurious disagreement between theory and experiment, as well as lack of experimental reproducibility.

4.4.4 Scattering Matrix

We assume that the series expansion (4.45) of the scattered field is uniformly convergent. Therefore, we can terminate the series after n_c terms and the resulting error will be arbitrarily small for all kr if n_c is sufficiently large. If, in addition, $kr \gg n_c^2$, we may substitute the asymptotic expressions (4.42) and (4.44) in the truncated series; the resulting transverse components of the scattered electric field are

$$E_{s\theta} \sim E_0 \frac{e^{ikr}}{-ikr} \cos\phi \, S_2(\cos\theta),$$

$$E_{s\phi} \sim -E_0 \frac{e^{ikr}}{-ikr} \sin\phi \, S_1(\cos\theta),$$

where

$$S_1 = \sum_n \frac{2n+1}{n(n+1)}(a_n\pi_n + b_n\tau_n),$$
$$S_2 = \sum_n \frac{2n+1}{n(n+1)}(a_n\tau_n + b_n\pi_n), \tag{4.74}$$

and the series are terminated after n_c terms. The relation between incident and scattered field amplitudes is therefore

$$\begin{pmatrix} E_{\parallel s} \\ E_{\perp s} \end{pmatrix} = \frac{e^{ik(r-z)}}{-ikr} \begin{pmatrix} S_2 & 0 \\ 0 & S_1 \end{pmatrix} \begin{pmatrix} E_{\parallel i} \\ E_{\perp i} \end{pmatrix}. \tag{4.75}$$

We can show from (4.25) that

$$\pi_n(1) = \tau_n(1) = \left.\frac{dP_n}{d\mu}\right|_{\mu=1}.$$

But P_n satisfies the differential equation (4.4), from which, together with $P_n(1) = 1$, it follows that

$$\pi_n(1) = \tau_n(1) = \frac{n(n+1)}{2}.$$

Thus, in the forward direction ($\theta = 0°$)

$$S_2(0°) = S_1(0°) = S(0°) = \tfrac{1}{2}\sum_n (2n+1)(a_n + b_n),$$

which when substituted in the optical theorem (3.24) yields the extinction cross section (4.62):

$$C_{\text{ext}} = \frac{4\pi}{k^2}\,\text{Re}\{S(0°)\}. \tag{4.76}$$

The relation between incident and scattered Stokes parameters follows from (4.75):

$$\begin{pmatrix} I_s \\ Q_s \\ U_s \\ V_s \end{pmatrix} = \frac{1}{k^2 r^2} \begin{pmatrix} S_{11} & S_{12} & 0 & 0 \\ S_{12} & S_{11} & 0 & 0 \\ 0 & 0 & S_{33} & S_{34} \\ 0 & 0 & -S_{34} & S_{33} \end{pmatrix} \begin{pmatrix} I_i \\ Q_i \\ U_i \\ V_i \end{pmatrix}, \tag{4.77}$$

$$S_{11} = \tfrac{1}{2}\left(|S_2|^2 + |S_1|^2\right), \qquad S_{12} = \tfrac{1}{2}\left(|S_2|^2 - |S_1|^2\right),$$

$$S_{33} = \tfrac{1}{2}(S_2^* S_1 + S_2 S_1^*), \qquad S_{34} = \frac{i}{2}(S_1 S_2^* - S_2 S_1^*).$$

Only three of these four matrix elements are independent: $S_{11}^2 = S_{12}^2 + S_{33}^2 + S_{34}^2$.

If the incident light is 100% polarized *parallel* to a particular scattering plane (it makes no difference which scattering plane), the Stokes parameters of the scattered light are

$$I_s = (S_{11} + S_{12})I_i, \qquad Q_s = I_s, \qquad U_s = V_s = 0,$$

where we have omitted the factor $1/k^2r^2$. Thus, the scattered light is also 100% polarized parallel to the scattering plane. We denote by $i_{\parallel}$ the scattered irradiance per unit incident irradiance given that the incident light is polarized parallel to the scattering plane:

$$i_{\parallel} = S_{11} + S_{12} = |S_2|^2.$$

If the incident light is polarized *perpendicular* to the scattering plane, the Stokes parameters of the scattered light are

$$I_s = (S_{11} - S_{12})I_i, \qquad Q_s = -I_s, \qquad U_s = V_s = 0.$$

Thus, the scattered light is also polarized perpendicular to the scattering plane. We denote by $i_{\perp}$ the scattered irradiance per unit incident irradiance given that the incident light is polarized perpendicular to the scattering plane:

$$i_{\perp} = S_{11} - S_{12} = |S_1|^2.$$

If the incident light is *unpolarized*, the Stokes parameters of the scattered light are

$$I_s = S_{11}I_i, \qquad Q_s = S_{12}I_i, \qquad U_s = V_s = 0.$$

The ratio

$$P = -\frac{S_{12}}{S_{11}} = \frac{i_{\perp} - i_{\parallel}}{i_{\perp} + i_{\parallel}} \tag{4.78}$$

is such that $|P| \leq 1$; if P is *positive*, the scattered light is partially polarized *perpendicular* to the scattering plane; if P is *negative*, the scattered light is partially polarized *parallel* to the scattering plane; the degree of polarization is $|P|$. Regardless of the size and composition of the sphere, $P(0°) = P(180°) = 0$.

If the incident light is *obliquely* polarized at an angle of 45° to the scattering plane, the scattered light will, in general, be *elliptically* polarized, although the azimuth of the vibration ellipse need not be 45°. The amount of rotation of the azimuth, as well as the ellipticity, depends not only on the particle characteristics but also on the direction in which the light is scattered.

Table 4.1 Scattering Coefficients for a Water Droplet in Air with Size Parameter $x = 3$ and Complex Refractive Index $m = 1.33 + i10^{-8}$

n	$\frac{2n+1}{n(n+1)}$	a_n	b_n
1	$\frac{3}{2}$	$5.1631 \times 10^{-1} - i4.9973 \times 10^{-1}$	$7.3767 \times 10^{-1} - i4.3990 \times 10^{-1}$
2	$\frac{5}{6}$	$3.4192 \times 10^{-1} - i4.7435 \times 10^{-1}$	$4.0079 \times 10^{-1} - i4.9006 \times 10^{-1}$
3	$\frac{7}{12}$	$4.8467 \times 10^{-2} - i2.1475 \times 10^{-1}$	$9.3553 \times 10^{-3} - i9.6269 \times 10^{-2}$
4	$\frac{9}{20}$	$1.0346 \times 10^{-3} - i3.2148 \times 10^{-2}$	$6.8810 \times 10^{-5} - i8.2949 \times 10^{-3}$
5	$\frac{11}{30}$	$9.0375 \times 10^{-6} - i3.0062 \times 10^{-3}$	$2.8309 \times 10^{-7} - i5.3204 \times 10^{-4}$

4.4.5 An Example of Angle-Dependent Scattering

As an example of angle-dependent scattering by a sphere we have chosen a water droplet with size parameter $x = 3$ illuminated by visible light of wavelength 0.55 μm. At this wavelength the complex refractive index of water is $1.33 + i10^{-8}$; $x = 3$ corresponds to a droplet radius of about 0.26 μm. The first five scattering coefficients for this particle are given in Table 4.1, from which it is clear that the first two or three functions π_n and τ_n determine the angular dependence of the scattering.

The results of computations using the program of Appendix A are shown in Fig. 4.9: linear polar plots of $i_\perp$ and $i_\parallel$ in part *a*; the logarithms of $i_\perp$ and $i_\parallel$ in *b*; and the polarization (4.78) in *c*; in all three sets of curves the independent

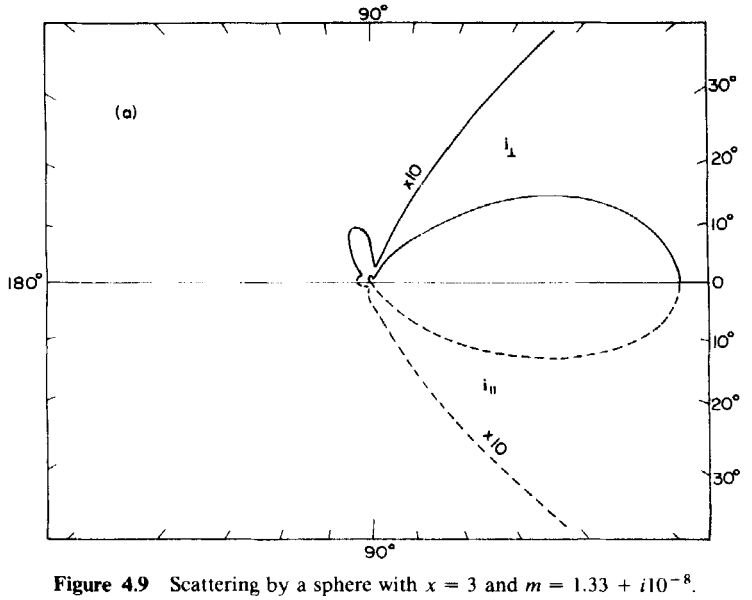

Figure 4.9 Scattering by a sphere with $x = 3$ and $m = 1.33 + i10^{-8}$.

variable is the scattering angle θ. Perhaps the most important point to note is that the scattering is highly peaked in the forward direction. This is seen most strikingly in the linear polar plot of part *a*. The small scattering lobes for $\theta > 90°$ are almost imperceptible compared with the strong forward-scattering lobes; indeed, for the backscattering lobes to be seen at all requires that we magnify the polar plots by a factor of 10. The scattered irradiance in the forward direction is more than 100 times greater than that in the backward direction; such directional asymmetry becomes even more pronounced as the size parameter increases, to the point that it is of little value to display scattering diagrams in a linear fashion. Our intent in showing this one polar plot is to emphasize the predominance of forward scattering even for rather small spheres—a 0.26-μm water droplet is so small as to be unheard of in clouds.

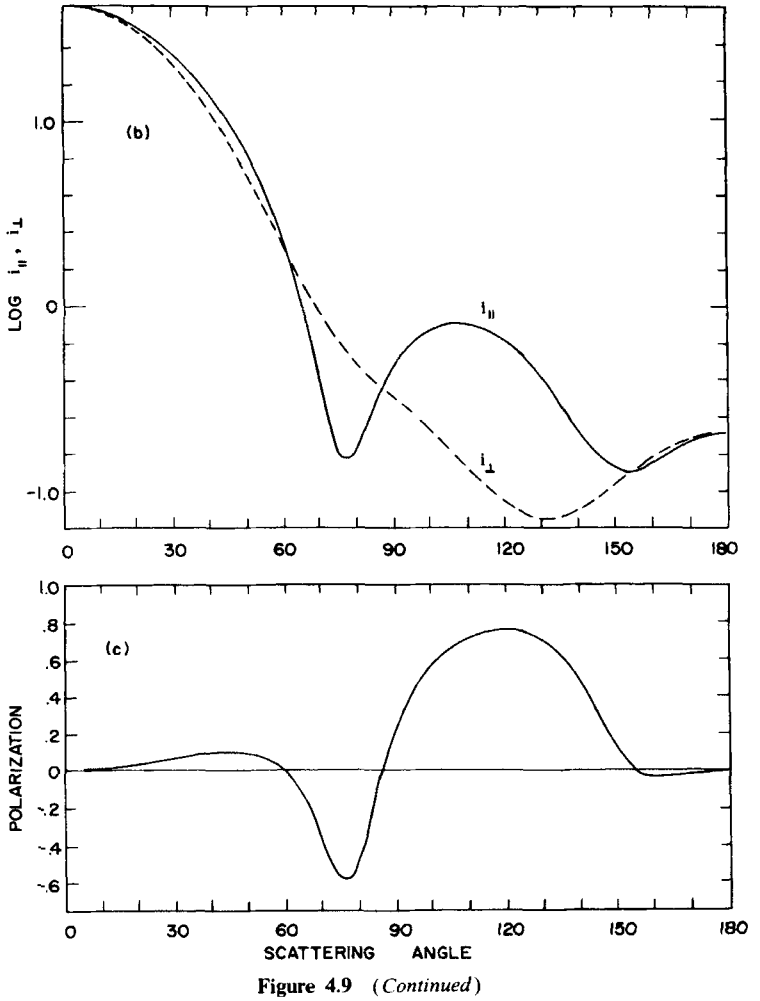

Figure 4.9 (*Continued*)

We encounter the consequences of strong forward scattering almost every day. An evening drive toward a bright setting sun can be a blinding experience, even if the direct sunlight is blocked by the sun visor, because of intense forward scattering by particles in the atmosphere and on the windshield. This is easily remedied by driving in the opposite direction—180° scattering is orders of magnitude less intense—but this solution usually has little practical appeal. In a similar way, night driving in fog or with a dirty windshield can be difficult: light from oncoming automobile headlights is scattered in the forward direction by fog droplets or particles to produce bothersome glare.

4.4.6 Integrated Extinction: A Sum Rule

We showed in Section 2.3 that the real and imaginary parts of the electric susceptibility are connected by the dispersion relations (2.36) and (2.37). This followed as a consequence of the linear causal relation between the electric field and polarization together with the vanishing of $\chi(\omega)$ in the limit of infinite frequency ω. We also stated that, in general, similar relations are expected to hold for any frequency-dependent function that connects an output with an input in a linear causal way. An example is the amplitude scattering matrix (4.75): the scattered field is linearly related to the incident field. Moreover, this relation must be causal: the scattered field cannot precede in time the incident field that excited it. Therefore, the matrix elements should satisfy dispersion relations. In particular, this is true for the forward direction $\theta = 0°$. But $S(0°, \omega)$ does not have the required asymptotic behavior: it is clear from the diffraction theory approximation (4.73) that for sufficiently large frequencies, $S(0°, \omega)$ is proportional to ω^2. Nevertheless, only minor fiddling with S makes it behave properly: the function

$$F(\omega) = \frac{S(0°, \omega)}{\omega^2} - \frac{a^2}{2c^2}$$

vanishes in the limit of infinite frequency; c is the speed of light *in vacuo* and we have taken the sphere to be in free space for convenience. When the domain of definition is extended to the complex $\tilde{\omega}$ plane, F is analytic in its upper half because of the analyticity of S; F also satisfies the same crossing condition as χ: $F(-\omega) = F^*(\omega)$. Therefore, the real and imaginary parts of $F = F' + iF''$ are connected by the integral relations (2.36) and (2.37):

$$F'(\omega) = \frac{2}{\pi} P \int_0^\infty \frac{\Omega F''(\Omega)}{\Omega^2 - \omega^2} d\Omega, \qquad F''(\omega) = \frac{-2\omega}{\pi} P \int_0^\infty \frac{F'(\Omega)}{\Omega^2 - \omega^2} d\Omega.$$

From these relations, the optical theorem (4.76), and (2.51) it follows that

$$2\pi^2 c^2 \frac{\mathrm{Im}\{S(0^0, \omega)\}}{\omega^3} = -P \int_0^\infty \frac{C_{\mathrm{ext}}(\Omega)}{\Omega^2 - \omega^2} d\Omega. \tag{4.79}$$

It is easy to show from (5.4) that for sufficiently small frequencies the forward scattering matrix element is given by

$$S(0^0, \omega) = -i\frac{\omega^3}{c^3}\frac{\epsilon(\omega) - 1}{\epsilon(\omega) + 2}\, a^3,$$

where the dielectric function $\epsilon = m^2$ is the permittivity of the particle relative to that of free space. Therefore, the limit of (4.79) as ω approaches zero is

$$\frac{2\pi^2 a^3}{c} \lim_{\omega \to 0} \operatorname{Im}\left\{ i\frac{\epsilon(\omega) - 1}{\epsilon(\omega) + 2} \right\} = \int_0^\infty \frac{C_{\text{ext}}(\Omega)}{\Omega^2} d\Omega. \tag{4.80}$$

This sum rule for extinction is written more compactly if we transform the integration variable from frequency to wavelength and assume that the static dielectric function is real and finite:

$$\int_0^\infty C_{\text{ext}}(\lambda)\, d\lambda = 4\pi^3 a^3 \frac{\epsilon(0) - 1}{\epsilon(0) + 2}. \tag{4.81}$$

Some rather remarkable conclusions follow from (4.81): although the dependence of C_{ext} on particle radius at a given wavelength may be quite complicated, the integrated extinction is merely proportional to the particle volume. Moreover, the optical properties of the particle enter into the integrated extinction only through the *static* dielectric function; the greater it is, the greater will be the integrated extinction. Thus, regardless of particle composition, we have an upper limit to integrated extinction:

$$\int_0^\infty C_{\text{ext}}(\lambda)\, d\lambda \leq 4\pi^3 a^3.$$

The sum rule (4.81) for extinction was first obtained by Purcell (1969) in a paper which we belive has not received the attention it deserves. Our path to this sum rule is different from that of Purcell's but we obtain essentially the same results. Purcell did not restrict himself to spherical particles but considered the more general case of spheroids. Regardless of the shape of the particle, however, it is plausible on physical grounds that integrated extinction should be proportional to the volume of an arbitrary particle, where the proportionality factor depends on its shape and static dielectric function.

4.4.7 Finite Beam Width

The expressions for the field scattered by a sphere were obtained under the assumption that the beam is infinite in lateral extent; such beams, however, are

difficult to produce in the laboratory. Nevertheless, it is physically plausible that scattering and absorption by any particle will be independent of the extent of the beam provided that it is large compared with the particle size; that is, the particle is completely bathed in the incident light. Our physical intuition is bolstered by the analysis of Tsai and Pogorzelski (1975), who obtained exact expressions for the field scattered by a sphere when the incident beam is cylindrically symmetric with a finite cross section. Their calculations of the angular dependence of the light scattered by a conducting sphere show no difference between infinite and finite beams provided that the beam radius is about 10 times larger than the sphere radius. In most scattering experiments, even those using highly collimated laser beams, this condition will certainly be satisfied. Thus, we are usually justified in ignoring finite beam width.

4.4.8 Charged Sphere

We have also assumed that the particle carries no net surface charge. This assumption, although not explicitly stated, is implicit in the boundary conditions (3.7). However, naturally occurring charged particles are not uncommon: water droplets formed in ocean sprays, water droplets and ice crystals in thunderstorms, drifting snow, and dust can be electrically charged; it is also believed that interstellar grains are charged (Spitzer, 1948). Thus, we are naturally led to the question: Does a particle that carries a physically realistic net charge scatter electromagnetic waves in any manner that is observably different from that of an identical uncharged particle? In an attempt to answer this question, Bohren and Hunt (1977) considered the problem of scattering by a sphere in which the conditions

$$(\mathbf{E}_2 - \mathbf{E}_1) \times \hat{\mathbf{e}}_r = 0, \qquad (\mathbf{H}_2 - \mathbf{H}_1) \times \hat{\mathbf{e}}_r = \mathbf{K},$$

where $\mathbf{K}$ is the surface current density of excess surface charge, were imposed at the boundary between particle and surrounding medium. If it is assumed that $\mathbf{K} = \sigma_s \mathbf{E}_{1t}$, where σ_s is a phenomenological surface conductivity and $\mathbf{E}_{1t}$ is the tangential field at the surface of the sphere, the coefficients of the scattered field can be obtained in a manner similar to that for an uncharged sphere. Obtaining the mathematical *form* of the scattering coefficients is easy enough; the difficulties arise when one tries to make *quantitative* conclusions in the absence of either measured values of σ_s or suitable microscopic theories. On the basis of a simple microscopic theory of free excess surface charges, Bohren and Hunt concluded that surface charges on metallic particles small compared with the wavelength do not appreciably affect the extinction cross section. However, a full understanding of scattering by charged particles awaits a satisfactory treatment of σ_s. In the interim, we shall assume, in the absence of evidence to the contrary, that surface charges on a particle only slightly perturb its scattering and absorbing properties.

4.5 ASYMMETRY PARAMETER AND RADIATION PRESSURE

The asymmetry parameter, which was defined in Section 3.4 as the average cosine of the scattering angle, depends, in general, on the polarization state of the incident light. However, the asymmetry parameter for a spherical particle is clearly independent of polarization and is given by

$$k^2 C_{sca}\langle \cos\theta \rangle = \pi \int_{-1}^{1} (|S_1|^2 + |S_2|^2)\mu \, d\mu,$$

where $\mu = \cos\theta$ and

$$|S_1|^2 + |S_2|^2 = \sum_n \sum_m \frac{2n+1}{n(n+1)} \frac{2m+1}{m(m+1)} \left[(a_n a_m^* + b_n b_m^*)(\tau_n \tau_m + \pi_n \pi_m) \right.$$

$$\left. + (a_n b_m^* + a_m^* b_n)(\tau_n \pi_m + \pi_n \tau_m) \right].$$

Therefore, to obtain the asymmetry parameter, we must evaluate the integrals

$$T_{nm}^{(1)} = \int_{-1}^{1} (\tau_n \pi_m + \pi_n \tau_m)\mu \, d\mu, \qquad T_{nm}^{(2)} = \int_{-1}^{1} (\tau_n \tau_m + \pi_n \pi_m)\mu \, d\mu.$$

The first of these integrals can be written in the form

$$T_{nm}^{(1)} = \int_0^{\pi} \left(\frac{dP_m^1}{d\theta} P_n^1 + P_m^1 \frac{dP_n^1}{d\theta} \right) \cos\theta \, d\theta$$

and integrated by parts to yield

$$T_{nm}^{(1)} = \delta_{nm} \frac{2n(n+1)}{2n+1},$$

where we have used the orthogonality of the P_n^1 (4.7). It follows from (4.48) that $\tau_n \tau_m + \pi_n \pi_m$ is an even function of μ if $m + n$ is even; therefore, $T_{nm}^{(2)}$ vanishes unless $m = n \pm p$, where $p = 1, 3, \ldots$. By using the recurrence relations

$$\tau_n = n\pi_{n+1} - (n+1)\mu\pi_n, \qquad \tau_n = n\mu\pi_n - (n+1)\pi_{n-1}$$

we can show that

$$\mu\tau_n = \frac{\pi_n}{n(n+1)} + \frac{n^2 \tau_{n+1}}{(n+1)(2n+1)} + \frac{(n+1)^2}{n(2n+1)} \tau_{n-1},$$

$$\mu\pi_n = \frac{\tau_n}{n(n+1)} + \frac{n^2 \pi_{n+1}}{(n+1)(2n+1)} + \frac{(n+1)^2}{n(2n+1)} \pi_{n-1},$$

from which, together with (4.24) and (4.26), it follows that

$$T_{nm}^{(2)} = \begin{cases} \dfrac{2n^2(n+1)(n+2)^2}{(2n+1)(2n+3)} & \text{if } m = n+1 \\ \dfrac{2n(n+1)^2(n-1)^2}{(2n+1)(2n-1)} & \text{if } m = n-1 \\ 0 & \text{if } m \neq n \pm 1 \end{cases}$$

Therefore, the asymmetry parameter is given by

$$Q_{\text{sca}}\langle\cos\theta\rangle = \frac{4}{x^2}\left[\sum_n \frac{n(n+2)}{n+1}\,\text{Re}\{a_n a_{n+1}^* + b_n b_{n+1}^*\} + \sum_n \frac{2n+1}{n(n+1)}\,\text{Re}\{a_n b_n^*\}\right].$$

In addition to energy, light carries *momentum*; therefore, a beam that interacts with a particle will exert a force on the particle, called *radiation pressure*. The momentum flux of a plane, homogeneous wave with phase velocity v is $\mathbf{S}/v$. If we now adopt the viewpoint that a beam of light consists of a stream of photons, it is physically reasonable to assert that the photons absorbed by the particle transfer all their momentum to the particle and therefore exert a force in the direction of propagation. If we interpret C_{abs} as the effective area for absorption, the momentum transfer to the particle is proportional to $I_i C_{\text{abs}}$, where I_i is the irradiance of the incident beam. Now let us interpret C_{sca} as the effective area for scattering. The photons incident on this area are elastically scattered through some distribution of angles θ, and the net rate of momentum transfer in the direction of propagation is therefore proportional to $I_i C_{\text{sca}}(1 - \langle\cos\theta\rangle)$. Thus, the total rate of momentum transfer to the particle is proportional to $I_i(C_{\text{ext}} - C_{\text{sca}}\langle\cos\theta\rangle)$, and we may define the *efficiency for radiation pressure* Q_{pr} as

$$Q_{\text{pr}} = Q_{\text{ext}} - Q_{\text{sca}}\langle\cos\theta\rangle.$$

The derivation above of the efficiency for radiation pressure is heuristic; a rigorous derivation of this result, which was first obtained by Debye (1909), entails integrating the stress tensor of the electromagnetic field over a spherical surface surrounding the particle.

4.6 RADAR BACKSCATTERING CROSS SECTION

McDonald (1962) has described the definition of the *radar backscattering cross section* as "intrinsically awkward"; we heartily agree that it is awkward, but we

suggest that it is less intrinsically than unnecessarily so. There are several definitions extant, but none with the power to elicit a clear image of just what is meant *physically* by the concept. Perhaps the clearest statement of the definition has been given by Battan (1973, p. 30), whom we paraphrase here. Consider an arbitrary particle illuminated by a beam with irradiance I_i, which is taken to be x-polarized. It is clear from the steps leading to (3.26) that the quantity $I_i|\mathbf{X}(\theta, \phi)|^2/k^2$ is the amount of energy scattered into a unit solid angle about a particular direction (θ, ϕ), where $\mathbf{X}$ is the vector scattering amplitude for the particle. Now consider a hypothetical *isotropic* scatterer illuminated by the same beam, where the vector scattering amplitude $\mathbf{X}_{iso}$ is independent of direction and is taken to be equal to the scattering amplitude in the backscattering direction ($\theta = 180°$) for the particle of interest: $\mathbf{X}_{iso} = \mathbf{X}(180°)$. The total energy W_{sca} scattered in all directions by the hypothetical particle is therefore

$$W_{sca} = \frac{I_i 4\pi |\mathbf{X}_{iso}|^2}{k^2} = \frac{I_i 4\pi |\mathbf{X}(180°)|^2}{k^2}.$$

The backscattering cross section σ_b is then *defined* by

$$\begin{aligned} I_i \sigma_b &= W_{sca} = \frac{I_i 4\pi |\mathbf{X}(180°)|^2}{k^2}, \\ \sigma_b &= \frac{4\pi |\mathbf{X}(180°)|^2}{k^2}. \end{aligned} \tag{4.82}$$

It is the presence of the factor 4π in (4.82) that is the obstacle to interpreting σ_b; were it not for this factor, σ_b would merely be the differential scattering cross section for scattering into a unit solid angle around the backscattering direction. In fact, it is obvious from (3.14) and (3.21) that the signal received by a detector subtending a solid angle $\Delta\Omega$ at the particle is proportional to $I_i \Delta\Omega |\mathbf{X}(\theta, \phi)|^2/k^2$ for *all* scattering angles. In addition to causing problems of interpretation, the historical definition also leads to a needless paradox: the backscattering cross section for a sphere small compared with the wavelength is *greater* than the total scattering cross section (Section 5.1). This implies, at first glance, that a part is greater than the whole!

The traditional definition of the radar backscattering cross section can be stated clearly in a few words: it is just 4π times what it ought to be. We therefore counsel the reader to mentally delete the factor 4π in (4.82) and only reintroduce it as a sop to convention when necessary.

For a sphere, we have from (3.22), (4.48), and (4.74)

$$|\mathbf{X}(180°)|^2 = |S_2(180°)|^2 \cos^2\phi + |S_1(180°)|^2 \sin^2\phi,$$

$$S_2(180°) = -S_1(180°) = \tfrac{1}{2} \sum_n (2n + 1)(-1)^n (a_n - b_n).$$

Therefore, the *efficiency for backscattering* Q_b is

$$Q_b = \frac{\sigma_b}{\pi a^2} = \frac{1}{x^2}\left|\sum_n (2n+1)(-1)^n(a_n - b_n)\right|^2.$$

McDonald (1962) gave a physical derivation of the limiting value of Q_b as $x \to \infty$, which, because of its appealing simplicity, is worth repeating here. Consider a sphere of radius a, which is taken to be large compared with the wavelength so that geometrical optics is a good approximation (see Chapter 7 for more details). The sphere is sufficiently absorbing so that all rays that are not reflected at the first interface are absorbed within the sphere; thus, scattering (excluding the forward diffraction peak, which does not contribute to the backscattering cross section) is entirely the result of reflection. Consider all those reflected rays that are confined within a set of directions defined by a cone of half-angle 2Θ about the backward direction, where $\Theta \ll 1$ but is shown on an enlarged scale in Fig. 4.10. All the energy ΔW_{sca} scattered into the solid angle $\Delta\Omega = \pi(2\Theta)^2$ results from reflection of incident rays with angles of incidence between 0 and Θ. Because Θ is small, this scattered energy is approximately $\Delta W_{\text{sca}} = I_i \pi a^2 \Theta^2 R(0°)$, where $R(0°)$ is the reflectance at normal incidence (2.58). Therefore, the backscattering cross section is given by

$$I_i \sigma_b = \frac{4\pi \Delta W_{\text{sca}}}{\Delta\Omega} = \pi a^2 R(0°) I_i,$$

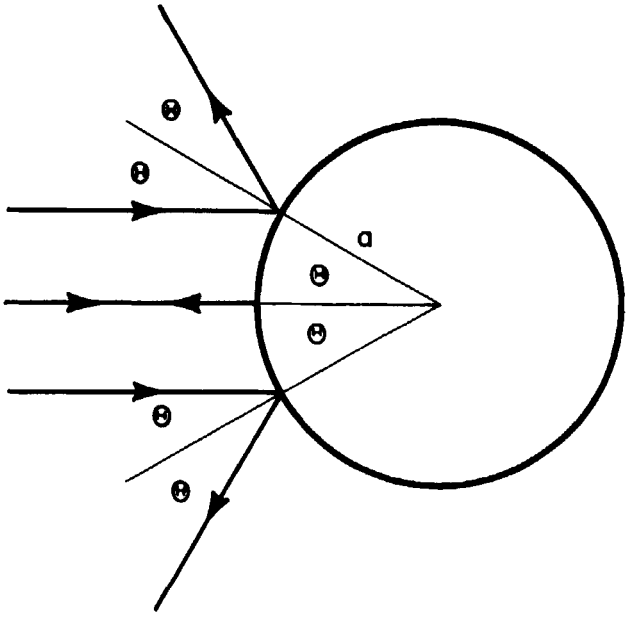

Figure 4.10 Backscattering by a large sphere in the geometrical optics approximation.

and the backscattering efficiency has the limiting value

$$\lim_{x \to \infty} Q_b = R(0°), \tag{4.83}$$

a surprisingly simple result which, because of the "peculiar nature" of the Q_b definition, is "less than obvious." Deirmendjian's calculations (1969, p. 40) of the backscattering efficiency for large metallic spheres supports this limiting value for Q_b. We emphasize that (4.83) is expected to be correct only if the sphere is absorbing so that internally reflected rays do not contribute to the backscattering. This in turn implies that for given x (provided, of course, that $x \gg 1$), $R(0°)$ will be a better approximation to the exact value the greater the absorption coefficient; the computations of Herman and Battan (1961) are consistent with this assertion.

Some of the more interesting applications of radar backscattering are given in *Radar Ornithology* by Eastwood (1967), in which one can find measured backscattering cross sections at 3-cm wavelength for pigeons, starlings, and house sparrows, together with calculations for "equivalent" spherical birds composed of water. It seems that Mie theory is sufficiently broad to embrace an unexpectedly large variety of objects.

4.7 THERMAL EMISSION

At temperatures above absolute zero, particles can emit as well as absorb and scatter electromagnetic radiation. Emission does not strictly fall within the bounds imposed in the first chapter; it is more akin to such phenomena as luminescence than to elastic scattering. However, because of the relation between emission and absorption, and because emission can be an important cooling mechanism for particles, it seems appropriate to discuss, at least briefly, thermal emission by a sphere.

Consider an enclosure of dimensions large compared with any wavelengths under consideration, which is opaque but otherwise arbitrary in shape and composition (Fig. 4.11). If the enclosure is maintained at a constant absolute temperature T, the equilibrium radiation field will be isotropic, homogeneous, and unpolarized (see Reif, 1965, p. 373 *et seq.* for a good discussion of equilibrium radiation in an enclosure). At any point the amount of radiant energy per unit frequency interval, confined to a unit solid angle about any direction, which crosses a unit area normal to this direction in unit time is given by the Planck function

$$\mathcal{P}_e = \frac{\hbar\omega^3}{4\pi^3 c^2} \frac{1}{\exp(\hbar\omega/k_B T) - 1},$$

where $\hbar = h/2\pi$, h is Planck's constant, c is the speed of light *in vacuo*, and k_B is Boltzmann's constant. $\mathcal{P}_e$ (or a similar expression) is sometimes referred to as

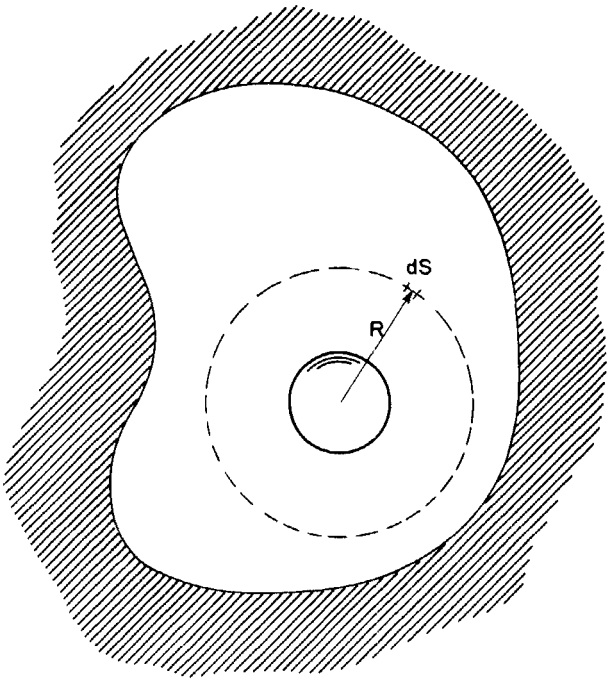

Figure 4.11 An enclosure, spherical particle, and radiation field in thermodynamic equilibrium.

the "blackbody" radiation distribution function. But the physical significance of the Planck function is that it is the distribution of radiation in equilibrium with matter; it does not require for its realization the existence of hypothetical "perfectly black" bodies. Indeed, as we shall see, rigid adherence to the notion of a perfect absorber leads to a needless paradox for small particles.

If a spherical particle is placed in the enclosure, then in equilibrium the distribution of radiation is unchanged. We may imagine that surrounding the particle there is a spherical surface of radius R, where R is much larger than the particle radius a, each element dS of which is the source of a nearly plane wave that illuminates the particle with irradiance $\mathcal{P}_e\, dS/R^2$ (Fig. 4.11). Therefore, the amount of energy absorbed per unit time by the particle is

$$\int_0^\infty \int_S \mathcal{P}_e C_{\text{abs}} \frac{dS}{R^2} d\omega = 4\pi \int_0^\infty \mathcal{P}_e C_{\text{abs}}\, d\omega.$$

In equilibrium the total power emitted by the particle must be equal to that absorbed:

$$\int_0^\infty W_e d\omega = 4\pi \int_0^\infty \mathcal{P}_e C_{\text{abs}} d\omega. \tag{4.84}$$

W_e is the power in a unit frequency interval, which by symmetry is emitted

uniformly in all directions. We define the *emissivity* e as the ratio of the power emitted by the particle to the power emitted by a particle that emits according to the Planck function:

$$e = \frac{W_e}{4\pi^2 a^2 \mathcal{P}_e}. \tag{4.85}$$

It follows from (4.84) and (4.85) that

$$\int_0^\infty \mathcal{P}_e(Q_{\text{abs}} - e)\, d\omega = 0. \tag{4.86}$$

A *sufficient* condition that (4.86) be satisfied is

$$Q_{\text{abs}} = e, \tag{4.87}$$

which may be interpreted as Kirchhoff's law for emission and absorption by an arbitrary spherical particle. However, it is not *necessary* that (4.87) hold in order for the energy of the particle to be conserved: an excess of emission over absorption at some frequencies could be balanced by an excess of absorption over emission at other frequencies. To show that $Q_{\text{abs}} = e$ is also necessary requires invoking the principle of detailed balance, a thorough discussion of which is beyond the scope of this book. Briefly stated, however, detailed balance is a consequence of time-reversal symmetry and requires that the probability of any process be equal to the probability of the reverse process (Reif, 1965, p. 384). A lengthy and rigorous derivation of (4.87) has been given by Kattawar and Eisner (1970), who solved the field equations for a homogeneous isothermal sphere with a fluctuating electric polarization.

Equation (4.87) was obtained under the assumption of strict thermodynamic equilibrium between the particle and the surrounding radiation field; that is, the particle at temperature T is embedded in a radiation field characterized by the same temperature. However, we are almost invariably interested in applying (4.87) to particles that are not in thermodynamic equilibrium with the surrounding radiation. For example, if the only mechanisms for energy transfer are radiative, then a particle illuminated by the sun or another star will come to constant temperature when emission balances absorption; but the particle's steady temperature will not, in general, be the same as that of the star. The validity of Kirchhoff's law for a body in a nonequilibrium environment has been the subject of some controversy. However, from the review by Baltes (1976) and the papers cited therein, it appears that questions about the validity of Kirchhoff's law are merely the result of different definitions of emission and absorption, and we are justified in using (4.87) for particles under arbitrary illumination.

We shall occasionally encounter spherical particles with absorption efficiencies greater than 1, sometimes much greater (see, e.g., Chapter 12). But if

Q_{abs} can be greater than 1, the emissivity can be greater than 1, which treads heavily on deep-seated prejudices about the upper limit a proper emissivity can assume; at first glance, an emissivity greater than 1 implies that the particle emits more than a "perfectly black particle." But what is a perfectly black particle? The standard definition of a perfect blackbody is that it absorbs all the light that is *incident on it*. The key phrase here is italicized; the notion of light geometrically incident on a body is a concept from geometrical optics, which fails to be valid for particles with dimensions comparable to or less than the wavelength. This was recognized by Planck (1913), who stated that "throughout the following discussion it will be assumed that the... radii of curvature of all surfaces under consideration are large compared with the wavelengths of the rays considered." According to Baltes (1976), Kirchhoff was also well aware of the restrictions on his derivations. Unfortunately, as so often happens in physics, each successive author in a chain extending from the source of a theory tends to omit more of the fine print underlying its validity. When a "paradox" is inevitably uncovered, brickbats are unfairly hurled at the theory when their proper target is those who uncritically use it in a state of blissful ignorance about its limitations.

We shall show in Section 7.1 that the absorption efficiency, and hence the emissivity, of a sufficiently large absorbing sphere is not greater than 1. Thus, when the sphere radius is much larger than the wavelength, the definition of particle emissivity (4.85) is consonant with elementary notions about the emissivity of a body. It is also interesting to note that if particles with individual emissivities greater than 1 are strewn onto a large substrate, the resulting emissivity of the composite system is not greater than 1.

4.8 COMPUTATION OF SCATTERING COEFFICIENTS AND CROSS SECTIONS

To obtain quantitative results from the Mie theory it might seem that we are faced with a straightforward task: we need merely calculate the scattering coefficients a_n and b_n together with the angular functions π_n and τ_n and sum the series (4.61) and (4.62) for the cross sections and (4.74) for the amplitude scattering matrix elements. However, the number of terms required for convergence can be quite large: a rough rule of thumb is that about x terms are sufficient (see, e.g., Table 4.1). Thus, if we were interested in investigating the rainbow—a visible scattering phenomenon familiar to all except perhaps inhabitants of the Atacama desert—we would need to sum about 12,000 terms assuming a water droplet radius of 1 mm. Such a calculation clearly requires more than just patience, pencil, pad of paper, and pocket calculator. Even for smaller particles the number of calculations can be painfully large. Indeed, until the advent of high-speed digital computers, scattering calculations were laborious, boring, and time consuming; and the literature on scattering as recently as a decade ago tended to be dominated by papers presenting numerical results for special cases. Although computers can greatly reduce the time required to sum series, there are problems inherent in the computation of

the scattering coefficients themselves; a_n and b_n are rather complicated functions of the spherical Bessel functions and their derivatives, the arguments of which are, in general, complex. Fortunately, the Bessel functions satisfy simple recurrence relations, (4.11) and (4.12), and, moreover, the first few orders are elementary trigonometric functions. We might therefore be tempted to assume that we could bootstrap our way forward by calculating Bessel functions of arbitrary order from the functions of the two preceding orders beginning with $n = 2$. Such would indeed be possible with a perfect computer at hand. Perfection is not of this world, however, and the *roundoff error* associated with the unavoidable representation of a number with an infinite number of digits by one with a finite number can accumulate in such a way as to yield incorrect results. There is not a unanimity of opinion about the conditions under which roundoff error accumulation can be a problem; this is most likely a consequence of different word lengths at various computer facilities, the fact that most people are usually interested in a limited range of sizes and optical properties, together with the unfortunate human tendency to generalize too readily on the basis of limited experience. However, there does seem to be common agreement that the *form* (4.56) and (4.57) of the scattering coefficients is not the one best suited for computations.

Aden (1951) was apparently the first to introduce the *logarithmic derivative*

$$D_n(\rho) = \frac{d}{d\rho} \ln \psi_n(\rho)$$

in the context of computing scattering coefficients for a sphere. We may therefore recast (4.56) and (4.57) in the form

$$\begin{aligned} a_n &= \frac{[D_n(mx)/m + n/x]\psi_n(x) - \psi_{n-1}(x)}{[D_n(mx)/m + n/x]\xi_n(x) - \xi_{n-1}(x)}, \\ b_n &= \frac{[mD_n(mx) + n/x]\psi_n(x) - \psi_{n-1}(x)}{[mD_n(mx) + n/x]\xi_n(x) - \xi_{n-1}(x)}, \end{aligned} \tag{4.88}$$

where we have used the recurrence relations

$$\psi_n'(x) = \psi_{n-1}(x) - \frac{n\psi_n(x)}{x}, \qquad \xi_n'(x) = \xi_{n-1}(x) - \frac{n\xi_n(x)}{x}$$

to eliminate ψ_n' and ξ_n'. Equations (4.88) are just *one* out of many possible ways of rewriting the scattering coefficients in a form more suitable for computation. The logarithmic derivative satisfies the recurrence relation

$$D_{n-1} = \frac{n}{\rho} - \frac{1}{D_n + n/\rho} \tag{4.89}$$

as a consequence of the recurrence relations (4.11) and (4.12).

There are two possible schemes for calculating $D_n(mx)$ in (4.88): *upward recurrence* (higher orders are generated from lower orders) and *downward*

recurrence (lower orders are generated from higher orders). Kattawar and Plass (1967) have shown that D_n is numerically stable with respect to downward recurrence; that is, if e_n is the error in D_n, then the error in D_{n-1} generated from (4.89) is such that $|e_{n-1}| \ll |e_n|$. Thus, beginning with an estimate for D_n, where n is larger than the number of terms required for convergence, successively more accurate lower-order logarithmic derivatives can be generated by downward recurrence. The downward stability of D_n is a consequence of the downward stability of the spherical Bessel functions j_n (Abramowitz and Stegun, 1964, p. xiii). But j_n is just one of two linearly independent solutions to the second-order differential equation (4.8); the other solution y_n satisfies the same recurrence relations as j_n but is numerically stable with respect to *upward* recurrence. If one begins with j_0 and j_1, it is possible to calculate accurate values of successive j_n by upward recurrence—up to a point. Where that point is depends on the precision of the computer; no matter how great the precision, however, an upward recurrence scheme for j_n must eventually lead to grief. For it is y_n that is stable by upward recurrence, and any such scheme must eventually find its way onto the stable solution regardless of how recurrence is initialized.

In the light of the preceding paragraph it appears that the most conservative method for computing scattering coefficients is to compute D_n and j_n by downward recurrence and y_n by upward recurrence (recall that $\psi_n = \rho j_n$ and $\xi_n = \rho j_n + i\rho y_n$). This does not seem to be necessary, however, provided that one does not demand more scattering coefficients than are necessary for convergence of the cross sections. One occasionally encounters the assertion that computations of scattering coefficients can always be done using only upward recurrence. This may indeed be true for weakly or moderately absorbing spheres. However, following Dave (1968), we have convinced ourselves that an otherwise satisfactory upward recurrence program will generate negative cross sections for sufficiently high absorption ($k_1 x > 80$ seems to be a reasonable criterion). Therefore, the calculations in this book were obtained with a program in which $D_n(mx)$ is calculated by downward recurrence, $\xi_n(x)$ and $\psi_n(x)$ by upward recurrence. We do not claim that this program, the details of which are given in Appendix A, is the most accurate or the fastest way of calculating scattering coefficients; it has met our modest computational needs satisfactorily. The disadvantage of downward recurrence is that all the scattering coefficients must be computed and stored before summing the series for the matrix elements and cross sections. With upward recurrence the scattering coefficients are computed and successively added to the partial sums of the series; as a consequence, the storage requirements are usually much less than for downward recurrence. As computers grow ever larger, however, storage problems become less acute.

Wiscombe (1979, 1980) has recently discussed very thoroughly many of the problems encountered in computing scattering coefficients and has suggested techniques for greatly increasing the speed of such computations.

Caution: Even if D_n and j_n are calculated by downward recurrence and y_n by upward recurrence with as much precision as can be squeezed out of the largest

computer available, there may be traps for the unwary in unexplored regions of m–x space.

NOTES AND COMMENTS

In an interesting historical article, Logan (1965) cites many of the early papers on the problem of scattering by a sphere.

The most detailed observations of extinction by the atmospheric particles responsible for the blue suns and moons widely observed in September 1950 were made by Wilson (1951). Subsequently, his and other data were thoroughly analyzed by Penndorf (1953). More recently, Porch et al. (1973) concluded on the basis of observations made at remote locations that bluing is a rather common property of the background (i.e., nonurban) aerosol. An elementary discussion of the blue moon, together with instructions on how to demonstrate one with cigarette smoke, was given by Bohren and Brown (1981).

Brillouin (1949) discussed the extinction paradox in much more detail than we have done in this chapter.

Box and McKellar (1978) derived the sum rule (4.81) under the assumption of a constant refractive index and within the framework of the anomalous diffraction approximation of van de Hulst (1957, Chap. 11).